Chaotic motion analysis of fluid-conveying viscoelastic nanotubes

Ali Farajpour [a], Hamed Farokhi [b], Mergen H. Ghayesh [a*]

[a] *School of Mechanical Engineering, University of Adelaide, South Australia 5005, Australia,*
[b] *Department of Mechanical and Construction Engineering, Northumbria University, Newcastle upon Tyne NE1 8ST, UK*
[*] *Corresponding author: mergen.ghayesh@adelaide.edu.au*

Abstract

In the current analysis, an attempt is made to develop a nonlinear size-dependent fluid-structure interaction model for the chaotic motion of nanofluid-conveying nanotubes subject to an external excitation. The material properties of the nanotube are assumed to be viscoelastic. Size effects in both solid and fluid nanoscale parts are taken into consideration. In addition, the effects of both centripetal and Coriolis accelerations are incorporated in the model. Using Hamilton's principle, the nonlocal strain gradient elasticity and the Beskok-Karniadaki theory, the nonlinear size-dependent governing equation is derived. For developing a precise solution approach, Galerkin's procedure and a direct-time-integration method are eventually used. Different parameters of the nanosystem are taken into consideration to study the size-dependent chaotic motion of the viscoelastic nanotube conveying nanofluid subject to a harmonic excitation.

Keywords: Chaos; Fluid-conveying nanotubes; Internal energy loss; Nonlocal strain gradient model

1. Introduction

Fluid-solid interactions (FSI) at small-scale levels such as microscales and nanoscales, between micro/nanoscale structures (Ashoori Movassagh and Mahmoodi, 2013; Wang et al., 2011; Zhang et al., 2013) and micro/nanofluids, are important since these interactions can affect the mechanical behaviour of the whole small-scale system. For instance, it has been shown that flowing nanofluid through a carbon nanotube (CNT) can alter its vibration response as well as its instability behaviour (Yoon et al., 2005). Therefore, for better manufacturing different small-scale systems containing flowing fluid such as nanofluidics devices, FSI interactions should be investigated and understood comprehensively.

A considerable number of articles have been reported on the mechanical response of macro-scale pipes conveying fluid (Bahaadini and Saidi, 2018; Deng et al., 2017; Ghayesh et al., 2011; Liu et al., 2018; Sinir and Demir, 2015); the studies on nano-scale pipes conveying fluid are limited. Since multiscale models are computationally costly and experimental techniques need much effort and skill, some theoretical models have been also developed. Among various theoretical models, the couple stress one (Ma et al., 2008; Şimşek and Reddy, 2013) has been mostly employed for microscale structures conveying fluid and the nonlocal theory (Aydogdu, 2014; Sudak, 2003) has been used for fluid-conveying nanoscale systems. In this paper, a novel nonlinear model which is capable of covering different sizes is applied via nonlocal and strain gradient models (Li and Hu, 2015).

Using the nonlocal theory, Wang (Wang, 2009) examined the scale-dependent mechanics of tubular ultrasmall beams containing flowing fluid; they particularly studied

the vibration and stability characteristics of the ultrasmall system. Lee and Chang (Lee and Chang, 2009) employed the nonlocal theory to scrutinise the effect of an elastic medium on the vibration response of fluid-conveying single-walled CNTs. In addition, the time-dependent deformation of fluid-conveying curved CNTs was studied in Ref. (Xia and Wang, 2010). Size effects on the oscillation of non-uniform nanotubes containing fluid flow surrounded by a viscoelastic medium were also examined by Rafiei et al. (Rafiei et al., 2012). Furthermore, Zhen and Fang (Zhen and Fang, 2015) developed a scale-dependent nonlocal model for large amplitude vibration of fluid-conveying CNTs subject to an external excitation; the proposed model contained only one scale parameter. Rashidi et al. (Rashidi et al., 2012) presented a theoretical model for the vibration of nanofluid-conveying nanotubes; in their model, small-scale effects on the flowing nanofluid were taken into consideration. Li et al. (Li et al., 2016) obtained the linear critical velocities of fluid-conveying ultrasmall tubes employing the nonlocal strain gradient theory as a two-parameter scale-dependent model. Moreover, the influences of surface properties (Zhang and Meguid, 2016) and a magnetic field (Arani et al., 2016; Arani et al., 2015; Hosseini and Sadeghi-Goughari, 2016) on the mechanical response of nanotubes conveying fluid have been examined in the literature. More recently, the mechanical behaviours of fluid-conveying functionally graded nanotubes (Filiz and Aydogdu, 2015), boron nitride nanotubes (Arani et al., 2013a; Arani et al., 2013b), nanocomposite shells (Arani et al., 2017) and piezoelectric nanotubes (Saadatnia and Esmailzadeh, 2017) have been investigated via use of scale-dependent theoretical models.

The valuable studies in the above paragraph are not comprehensive in terms of size-dependent theoretical modelling. The majority of them include only one scale parameter, leading to a model limited to a small size range. In addition, few nonlinear models, in which only one eigenfunction was considered in solution procedures, were developed. In the present analysis, a size-dependent nonlinear fluid-structure interaction model is proposed for the bifurcation response of viscoelastic nanotubes containing nanofluid flow; this is for the first time. To better describe the size influence on the solid part of the nanosystem (the nanotube), a nonlocal strain gradient theory is applied. Moreover, to take into account the size influence on the nanofluid flow, a speed correction factor is used. Based on Hamilton's principle, the nonlinear motion equation of the nanofluid-conveying nanotube is extracted. Applying Galerkin's procedure and a direct-time-integration solver, the motion equation is numerically solved. Various nanosystem parameters are taken into account in order to examine the chaotic oscillations of nanofluid-conveying nanotubes with viscoelastic material properties.

2. Size-dependent modelling

Figure 1 illustrates a nanofluid-conveying nanoscale tube with clamped-clamped boundary conditions. The average diameter and length of the nanoscale tube are d and L, respectively. In addition, let us denote the modulus of elasticity, viscosity constant and Poisson's ratio of the solid part by E, η and v, respectively. The longitudinal and transverse time-dependent displacements of the mid-plane are also indicated by u and w, respectively.

The longitudinal component of the strain tensor can be expressed as (Ghayesh et al., 2016; Reddy and Pang, 2008)

$$\varepsilon_{xx} = \varepsilon_{xx}^{0} + z\kappa_{xx}^{0}, \tag{1}$$

where ε_{xx}^{0} and κ_{xx}^{0} are given by

$$\varepsilon_{xx}^{0} = \frac{\partial u}{\partial x} + \frac{1}{2}\left(\frac{\partial w}{\partial x}\right)^{2}, \quad \kappa_{xx}^{0} = -\frac{\partial^{2} w}{\partial x^{2}}. \tag{2}$$

In view of the Kelvin-Voigt scheme (Ghayesh, 2018a, b) together with the strain gradient and nonlocal models, the constitutive relation of the solid part can be written as (Lim et al., 2015)

$$\begin{aligned}\sigma_{xx}^{(t)} - \left(e_0 a\right)^2 \nabla^2 \sigma_{xx}^{(t)} &= E\left[\varepsilon_{xx}^{0} + z\kappa_{xx}^{0} - l_{sg}^{2}\nabla^2\left(\varepsilon_{xx}^{0} + z\kappa_{xx}^{0}\right)\right] \\ &+\eta\left[\frac{\partial \varepsilon_{xx}^{0}}{\partial t} + z\frac{\partial \kappa_{xx}^{0}}{\partial t} - l_{sg}^{2}\nabla^2\left(\frac{\partial \varepsilon_{xx}^{0}}{\partial t} + z\frac{\partial \kappa_{xx}^{0}}{\partial t}\right)\right].\end{aligned} \tag{3}$$

Here $\sigma_{xx}^{(t)}$ and ∇^2 represent the total longitudinal stress and the Laplacian operator, respectively (Farajpour et al., 2018a). The strain gradient and nonlocal parameters are, respectively, denoted by l_{sg} and $e_0 a$ in which e_0 and a represent the nonlocal calibration coefficient and the internal characteristic length, respectively. Let us denote the cross-sectional area and inertia moment of the nanotube by A and I, respectively. For convenience purposes, the stress resultants in the solid part of the fluid-conveying nanosystem are defined as

$$\left\langle N_{xx}, M_{xx}\right\rangle = \int_{A}\left\langle \sigma_{xx}^{(t)}, z\sigma_{xx}^{(t)}\right\rangle dA. \tag{4}$$

Using Eqs. (1)-(4), the stress resultants of the solid part are formulated as

$$N_{xx}-\left(e_0a\right)^2\nabla^2N_{xx}=A\left(1-l_{sg}^2\nabla^2\right)\left\{E\left[\frac{\partial u}{\partial x}+\frac{1}{2}\left(\frac{\partial w}{\partial x}\right)^2\right]+\eta\left(\frac{\partial^2u}{\partial t\partial x}+\frac{\partial w}{\partial x}\frac{\partial^2w}{\partial t\partial x}\right)\right\}, \tag{5}$$

$$M_{xx}-\left(e_0a\right)^2\nabla^2M_{xx}=-I\left(1-l_{sg}^2\nabla^2\right)\left(E\frac{\partial^2w}{\partial x^2}+\eta\frac{\partial^3w}{\partial t\partial x^2}\right). \tag{6}$$

The effects of zeroth-order and first-order stress nonlocalities are taken into consideration in the nonlocal strain gradient elasticity. Moreover, both viscoelastic and elastic stresses are simultaneously incorporated in the present model. In view of the nonlocal and strain gradient viscoelastic models, one can write (Lim et al., 2015)

$$\begin{Bmatrix}\sigma_{ij}^{(t)}\\ \sigma_{ij}^{(1)}\\ \sigma_{ij}^{(0)}\end{Bmatrix}=\begin{Bmatrix}\sigma_{ij(el)}^{(t)}\\ \sigma_{ij(el)}^{(1)}\\ \sigma_{ij(el)}^{(0)}\end{Bmatrix}+\begin{Bmatrix}\sigma_{ij(vis)}^{(t)}\\ \sigma_{ij(vis)}^{(1)}\\ \sigma_{ij(vis)}^{(0)}\end{Bmatrix}. \tag{7}$$

$$\begin{Bmatrix}\sigma_{ij}^{(t)}\\ \sigma_{ij(el)}^{(t)}\\ \sigma_{ij(vis)}^{(t)}\end{Bmatrix}=\begin{Bmatrix}\sigma_{ij}^{(0)}\\ \sigma_{ij(el)}^{(0)}\\ \sigma_{ij(vis)}^{(0)}\end{Bmatrix}-\nabla\begin{Bmatrix}\sigma_{ij}^{(1)}\\ \sigma_{ij(el)}^{(1)}\\ \sigma_{ij(vis)}^{(1)}\end{Bmatrix}, \tag{8}$$

in which $\sigma_{ij}^{(0)}$ and $\sigma_{ij}^{(1)}$ indicate the zeroth-order and first-order nonlocal stresses, respectively; ∇ stands for the gradient operator (Farajpour et al., 2018b); "*el*" and "*vis*" are used to indicate the elastic and viscoelastic stress segments, respectively. Using elastic and viscoelastic stresses, the variations of the elastic energy (U_{el}) and the work caused by the viscous stress (W_{vis}) are as

$$\delta U_{el}=\int_0^L\int_A\sigma_{xx(el)}^{(t)}\delta\varepsilon_{xx}dAdx+\left[\int_A\sigma_{xx(el)}^{(1)}\delta\varepsilon_{xx}dA\right]_0^L, \tag{9}$$

$$\delta W_{vis} = -\int_0^L \int_A \sigma_{xx(vis)}^{(t)} \delta\varepsilon_{xx} dA dx - \left[\int_A \sigma_{xx(vis)}^{(1)} \delta\varepsilon_{xx} dA \right]_0^L . \tag{10}$$

Incorporating the effects of the slip boundary condition on the internal wall of the nanotube (Rashidi et al., 2012), the variation of the total motion energy of the nanofluid-conveying nanosystem (δT_e) can be written as

$$\begin{aligned} \delta T_e = {} & m_{nt} \int_0^L \frac{\partial u}{\partial t} \delta \frac{\partial u}{\partial t} dx + m_{nf} \int_0^L \left(\kappa_{nf} U + \kappa_{nf} U \frac{\partial u}{\partial x} + \frac{\partial u}{\partial t} \right) \left(\kappa_{nf} U \delta \frac{\partial u}{\partial x} + \delta \frac{\partial u}{\partial t} \right) dx \\ & + m_{nt} \int_0^L \frac{\partial w}{\partial t} \delta \frac{\partial w}{\partial t} dx + m_{nf} \int_0^L \left(\kappa_{nf} U \frac{\partial w}{\partial x} + \frac{\partial w}{\partial t} \right) \left(\kappa_{nf} U \delta \frac{\partial w}{\partial x} + \delta \frac{\partial w}{\partial t} \right) dx, \end{aligned} \tag{11}$$

where *U* and *m* are respectively the nanofluid speed and the mass per unit length; "*nt*" and "*nf*" denote the nanotube and the nanofluid, respectively; κ_{nf} is a speed correction factor defined by (Beskok and Karniadakis, 1999)

$$\kappa_{nf} = \frac{U_{ave}^{s}}{U_{ave}^{ns}}, \tag{12}$$

where U_{ave}^{ns} and U_{ave}^{s} indicate the average nanofluid velocities for the no-slip and slip boundary conditions, respectively. According to the Beskok-Karniadaki theory, the speed correction factor is determined as (Beskok and Karniadakis, 1999)

$$\kappa_{nf} = \left(1 + \gamma Kn\right) \left[1 + \frac{4Kn}{1+Kn} \left(\frac{2-\sigma_v}{\sigma_v} \right) \right], \tag{13}$$

where σ_v is the tangential momentum accommodation constant. This constant is usually set to 0.7 for numerical calculations. *Kn* represents the Knudsen number defined as

$$Kn = \frac{\Lambda_p}{L_e}, \tag{14}$$

in which Λ_p and L_e are respectively the average molecular free path and an external characteristics dimension. In Eq. (13), γ is a constant coefficient given by (Rashidi et al., 2012)

$$\gamma = \frac{2\gamma_0}{\pi}\tan^{-1}\left[A\left(Kn\right)^B\right], \tag{15}$$

where

$$\gamma_0 = \lim_{Kn\to\infty}\gamma = \frac{64}{15\pi}. \tag{16}$$

In Eq. (15), *A* and *B* are constant coefficients; the former is set to 4 while the latter is equal to 0.4. It should be noticed that at nanoscale levels, no-slip boundary conditions are no longer valid. The speed correction factor takes into account the influences of slip boundary conditions on the mechanical behaviour of nanoscale tubes. This factor depends on the Knudsen number (*Kn*) as seen from Eq. (13). It has been shown that ignoring this factor (*Kn*=0) leads to overestimated results for the critical velocity corresponding to divergence (Rashidi et al., 2012). The work (W_F) caused by the external transverse excitation is as (Ghayesh et al., 2013a; Ghayesh et al., 2013b)

$$\delta W_F = F_1\int_0^L \cos\left(\omega t\right)\delta w\,\mathrm{d}x, \tag{17}$$

where F_1 and ω indicate the forcing amplitude and frequency, respectively. Now, employing Hamilton's principle given by (Ghayesh, 2018c; Ghayesh et al., 2014)

$$\int_{t_1}^{t_2}\delta\left(T_e + W_F - U_{el} + W_{vis}\right)\mathrm{d}t = 0, \tag{18}$$

one can obtain the nonlinear size-dependent governing equations as

$$\frac{\partial N_{xx}}{\partial x}=\left(m_{nt}+m_{nf}\right)\frac{\partial^2 u}{\partial t^2}+2\kappa_{nf}m_{nf}U\frac{\partial^2 u}{\partial t\partial x}+\left(\kappa_{nf}\right)^2 m_{nf}U^2\frac{\partial^2 u}{\partial x^2}, \tag{19}$$

$$\begin{aligned}&\frac{\partial^2 M_{xx}}{\partial x^2}+F_1\cos\left(\omega t\right)+\frac{\partial}{\partial x}\left(N_{xx}\frac{\partial w}{\partial x}\right)=\\&\left(m_{nt}+m_{nf}\right)\frac{\partial^2 w}{\partial t^2}+2\kappa_{nf}m_{nf}U\frac{\partial^2 w}{\partial t\partial x}+\left(\kappa_{nf}\right)^2 m_{nf}U^2\frac{\partial^2 w}{\partial x^2}.\end{aligned} \tag{20}$$

Neglecting inertia terms in the governing equation along the axial direction (i.e. Eq. (19)), and then using Eqs. (5) and (6) together with Eqs. (19) and (20), we have

$$\begin{aligned}&\left(EA-EAl_{sg}^2\nabla^2\right)\frac{\partial}{\partial x}\left[\frac{1}{2}\left(\frac{\partial w}{\partial x}\right)^2+\frac{\partial u}{\partial x}\right]\\&+\left(\eta A-\eta Al_{sg}^2\nabla^2\right)\frac{\partial}{\partial x}\left(\frac{\partial w}{\partial x}\frac{\partial^2 w}{\partial t\partial x}+\frac{\partial^2 u}{\partial t\partial x}\right)=0,\end{aligned} \tag{21}$$

$$\begin{aligned}&-EIl_{sg}^2\nabla^2\left(\frac{\partial^4 w}{\partial x^4}\right)+EI\frac{\partial^4 w}{\partial x^4}-\eta Il_{sg}^2\nabla^2\left(\frac{\partial^5 w}{\partial t\partial x^4}\right)+\eta I\frac{\partial^5 w}{\partial t\partial x^4}\\&-\frac{\partial}{\partial x}\left(N_{xx}\frac{\partial w}{\partial x}\right)+\left(e_0 a\right)^2\nabla^2\left[\frac{\partial}{\partial x}\left(N_{xx}\frac{\partial w}{\partial x}\right)\right]-F_1\cos\left(\omega t\right)=\\&-\left[\left(m_{nt}+m_{nf}\right)\frac{\partial^2 w}{\partial t^2}+2\kappa_{nf}m_{nf}U\frac{\partial^2 w}{\partial t\partial x}+\left(\kappa_{nf}\right)^2 m_{nf}U^2\frac{\partial^2 w}{\partial x^2}\right]\\&+\left(e_0 a\right)^2\nabla^2\left[\left(m_{nt}+m_{nf}\right)\frac{\partial^2 w}{\partial t^2}+2\kappa_{nf}m_{nf}U\frac{\partial^2 w}{\partial t\partial x}+\left(\kappa_{nf}\right)^2 m_{nf}U^2\frac{\partial^2 w}{\partial x^2}\right].\end{aligned} \tag{22}$$

Integrating Eq. (21) with respect to *x* leads to the following equation

$$\begin{aligned}&\left(EA-EAl_{sg}^2\nabla^2\right)\left[\frac{1}{2}\left(\frac{\partial w}{\partial x}\right)^2+\frac{\partial u}{\partial x}\right]\\&+\left(\eta A-\eta Al_{sg}^2\nabla^2\right)\left(\frac{\partial w}{\partial x}\frac{\partial^2 w}{\partial t\partial x}+\frac{\partial^2 u}{\partial t\partial x}\right)=C,\end{aligned} \tag{23}$$

in which *C* is an integration constant which is determined from the boundary conditions of the axial displacement as

$$C=\int_0^L\left[\frac{EA}{2L}\left(1-l_{sg}^2\nabla^2\right)\left(\frac{\partial w}{\partial x}\right)^2+\frac{\eta A}{L}\left(1-l_{sg}^2\nabla^2\right)\frac{\partial w}{\partial x}\frac{\partial^2 w}{\partial t\partial x}\right]dx. \tag{24}$$

Substituting the above equation (i.e. Eq. (24)) into Eq. (22), the final nonlinear size-dependent governing equation is obtained as

$$\begin{aligned}
&-EIl_{sg}^2\nabla^2\left(\frac{\partial^4 w}{\partial x^4}\right)+EI\frac{\partial^4 w}{\partial x^4}-\eta Il_{sg}^2\nabla^2\left(\frac{\partial^5 w}{\partial t\partial x^4}\right)+\eta I\frac{\partial^5 w}{\partial t\partial x^4}\\
&-\frac{A}{L}\left[\frac{\partial^2 w}{\partial x^2}-\left(e_0a\right)^2\nabla^2\left(\frac{\partial^2 w}{\partial x^2}\right)\right]\left(\frac{E}{2}\int_0^L\left(1-l_{sg}^2\nabla^2\right)\left[\left(\frac{\partial w}{\partial x}\right)^2\right]dx\right.\\
&\left.+\eta\int_0^L\left(1-l_{sg}^2\nabla^2\right)\left(\frac{\partial^2 w}{\partial t\partial x}\frac{\partial w}{\partial x}\right)dx\right)-F_1\cos\left(\omega t\right)=\\
&-\left[\left(m_{nt}+m_{nf}\right)\frac{\partial^2 w}{\partial t^2}+2\kappa_{nf}m_{nf}U\frac{\partial^2 w}{\partial t\partial x}+\left(\kappa_{nf}\right)^2m_{nf}U^2\frac{\partial^2 w}{\partial x^2}\right]\\
&+\left(e_0a\right)^2\nabla^2\left[\left(m_{nt}+m_{nf}\right)\frac{\partial^2 w}{\partial t^2}+2\kappa_{nf}m_{nf}U\frac{\partial^2 w}{\partial t\partial x}+\left(\kappa_{nf}\right)^2m_{nf}U^2\frac{\partial^2 w}{\partial x^2}\right].
\end{aligned} \tag{25}$$

For convenience during the numerical solution, let us consider the following dimensionless parameters and operators

$$\begin{aligned}
&\alpha=\frac{x}{L},\ \tilde{w}=\frac{w}{d},\ \chi_{nl}=\frac{e_0a}{L},\ \chi_{sg}=\frac{l_{sg}}{L},\ \tilde{A}=\frac{AL^2}{I},\\
&\tau=\frac{t}{L^2}\sqrt{\frac{EI}{m_{nt}+m_{nf}}},\ \tilde{m}=\frac{m_{nf}}{m_{nt}+m_{nf}},\ \tilde{U}=\sqrt{\frac{m_{nf}}{EI}}UL,\ \tilde{\nabla}^2=\frac{\partial^2}{\partial\alpha^2},\\
&s=\frac{L}{d},\ \tilde{F}_1=\frac{F_1L^4}{EId},\ \tilde{\eta}=\sqrt{\frac{EI}{m_{nt}+m_{nf}}}\frac{\eta}{EL^2},\ \tilde{\omega}=\sqrt{\frac{L^4\left(m_{nt}+m_{nf}\right)}{EI}}\omega.
\end{aligned} \tag{26}$$

In view of the above definitions, Eq. (25) can be rewritten as

$$
\begin{aligned}
&-\chi_{sg}^2\tilde{\nabla}^2\left(\frac{\partial^4\tilde{w}}{\partial\alpha^4}\right)+\frac{\partial^4\tilde{w}}{\partial\alpha^4}-\tilde{\eta}\chi_{sg}^2\tilde{\nabla}^2\left(\frac{\partial^5\tilde{w}}{\partial\tau\partial\alpha^4}\right)+\tilde{\eta}\frac{\partial^5\tilde{w}}{\partial\tau\partial\alpha^4}\\
&-\frac{\tilde{A}}{s^2}\left[\frac{\partial^2\tilde{w}}{\partial\alpha^2}-\chi_{nl}^2\tilde{\nabla}^2\left(\frac{\partial^2\tilde{w}}{\partial\alpha^2}\right)\right]\left(\frac{1}{2}\int_0^1\left(1-\chi_{sg}^2\tilde{\nabla}^2\right)\left[\left(\frac{\partial\tilde{w}}{\partial\alpha}\right)^2\right]d\alpha\right.\\
&\left.+\tilde{\eta}\int_0^1\left(1-\chi_{sg}^2\tilde{\nabla}^2\right)\left(\frac{\partial^2\tilde{w}}{\partial\tau\partial\alpha}\frac{\partial\tilde{w}}{\partial\alpha}\right)d\alpha\right)-\tilde{F}_1\cos\left(\tilde{\omega}\tau\right)=\\
&-\left[\frac{\partial^2\tilde{w}}{\partial\tau^2}+2\kappa_{nf}\sqrt{\tilde{m}}\tilde{U}\frac{\partial^2\tilde{w}}{\partial\tau\partial\alpha}+\left(\kappa_{nf}\right)^2\tilde{U}^2\frac{\partial^2\tilde{w}}{\partial\alpha^2}\right]\\
&+\chi_{nl}^2\tilde{\nabla}^2\left[\frac{\partial^2\tilde{w}}{\partial\tau^2}+2\kappa_{nf}\sqrt{\tilde{m}}\tilde{U}\frac{\partial^2\tilde{w}}{\partial\tau\partial\alpha}+\left(\kappa_{nf}\right)^2\tilde{U}^2\frac{\partial^2\tilde{w}}{\partial\alpha^2}\right].
\end{aligned}
\tag{27}
$$

To obtain the nonlinear dynamic characteristics of nanofluid-conveying viscoelastic nanotubes subject to external excitation loading, the nonlinear size-dependent (Gholipour et al., 2015) governing equation (i.e. Eq. (27)) is discretised. For this purpose, the non-dimensional transverse deflection ($\tilde{w}$) is expressed as

$$
\tilde{w}(\alpha,\tau)=\sum_{i=1}^{N_z}q_i(\tau)\Theta_i(\alpha),
\tag{28}
$$

where q_i and Θ_i are used to indicate the general coordinates and eigenfunctions of the nanosystem, respectively. Substituting Eq. (28) into Eq. (27) and applying Galerkin's procedure, the following set of equations is derived

$$
\begin{aligned}
&\sum_{i=1}^{N_z}\left(\int_0^1\Theta_k\Theta_i d\alpha\right)\frac{d^2q_i}{d\tau^2}+2\kappa_{nf}\sqrt{\tilde{m}}\tilde{U}\sum_{i=1}^{N_z}\left(\int_0^1\Theta_k\frac{d\Theta_i}{d\alpha}d\alpha\right)\frac{dq_i}{d\tau}\\
&+\left(\kappa_{nf}\right)^2\tilde{U}^2\sum_{i=1}^{N_z}\left(\int_0^1\Theta_k\frac{d^2\Theta_i}{d\alpha^2}d\alpha\right)q_i-\chi_{nl}^2\left[\sum_{i=1}^{N_z}\left(\int_0^1\Theta_k\frac{d^2\Theta_i}{d\alpha^2}d\alpha\right)\frac{d^2q_i}{d\tau^2}\right.\\
&\left.+2\kappa_{nf}\sqrt{\tilde{m}}\tilde{U}\sum_{i=1}^{N_z}\left(\int_0^1\Theta_k\frac{d^3\Theta_i}{d\alpha^3}d\alpha\right)\frac{dq_i}{d\tau}+\left(\kappa_{nf}\right)^2\tilde{U}^2\sum_{i=1}^{N_z}\left(\int_0^1\Theta_k\frac{d^4\Theta_i}{d\alpha^4}d\alpha\right)q_i\right]
\end{aligned}
$$

$$
\begin{aligned}
&+\sum_{i=1}^{N_z}\left(\int_0^1 \Theta_k \frac{d^4\Theta_i}{d\alpha^4} d\alpha\right) q_i - \chi_{sg}^2 \sum_{i=1}^{N_z}\left(\int_0^1 \Theta_k \frac{d^6\Theta_i}{d\alpha^6} d\alpha\right) q_i \\
&+\tilde{\eta}\left[\sum_{i=1}^{N_z}\left(\int_0^1 \Theta_k \frac{d^4\Theta_i}{d\alpha^4} d\alpha\right)\frac{dq_i}{d\tau} - \chi_{sg}^2 \sum_{i=1}^{N_z}\left(\int_0^1 \Theta_k \frac{d^6\Theta_i}{d\alpha^6} d\alpha\right)\frac{dq_i}{d\tau}\right] \\
&-\frac{\tilde{A}}{s^2}\left[\sum_{i=1}^{N_z}\left(\int_0^1 \Theta_k \frac{d^2\Theta_i}{d\alpha^2} d\alpha\right) q_i - \chi_{nl}^2 \sum_{i=1}^{N_z}\left(\int_0^1 \Theta_k \frac{d^4\Theta_i}{d\alpha^4} d\alpha\right) q_i\right] \times \\
&\left(\frac{1}{2}\int_0^1 \left\{\left(\sum_{i=1}^{N_z}\frac{d\Theta_i}{d\alpha} q_i\right)^2 - \chi_{sg}^2 \frac{d^2}{d\alpha^2}\left[\left(\sum_{i=1}^{N_z}\frac{d\Theta_i}{d\alpha} q_i\right)^2\right]\right\} d\alpha\right. \\
&\left.+\tilde{\eta}\int_0^1 \left[\sum_{i=1}^{N_z}\sum_{j=1}^{N_z} q_i \frac{dq_j}{d\tau}\frac{d\Theta_i}{d\alpha}\frac{d\Theta_j}{d\alpha} - \chi_{sg}^2 \frac{d^2}{d\alpha^2}\left(\sum_{i=1}^{N_z}\sum_{j=1}^{N_z}\frac{dq_j}{d\tau} q_i \frac{d\Theta_j}{d\alpha}\frac{d\Theta_i}{d\alpha}\right)\right] d\alpha\right) \\
&-\left(\int_0^1 \Theta_k d\alpha\right)\tilde{F}_1 \cos(\tilde{\omega}\tau) = 0,
\end{aligned}
\tag{29}
$$

To numerically solve the above set of equations, a direct-time-integration method is eventually applied. It should be noted that to precisely describe the nonlinear scale-dependent dynamic characteristics of nanofluid-conveying viscoelastic nanotubes subject to external excitation loading, eight eigenfunctions are taken into consideration.

3. Numerical results

The scale-dependent chaotic motion of viscoelastic nanotubes conveying nanofluid is investigated in the following. The elastic and geometric properties of the viscoelastic nanotube are, respectively, set to (E,ν, ρ_{nt})=(610 MPa,0.3,1024 kg/m^3) and (h,R_o,L)=(66 nm,290.5 nm, 20d_o) where ρ_{nt} and R_o denote the mass density and outer radius of the viscoelastic nanotube, respectively. The dimensionless parameters of the nanosystem are $\chi_{nl}=0.12$, $\chi_{sg}=0.04$, $\Xi=4006.941$, $\bar{M}=0.5915$, $s=20$ and $\eta^*=0.0005$. In addition, for

all cases, it is assumed that ω /ω_1=1.0 in which ω_1 stands for the fundamental natural frequency. For this viscoelastic nanotube, the critical flow speed corresponding to buckling is U_{cr}=4.13118.

Shown in Fig. 2 is the bifurcation response of the Poincaré section of the nanotube conveying nanofluid flow for a speed before the critical value (U =3.95<U_{cr}); the transverse deflection is plotted at x=0.45. The natural frequency is determined as ω_1= 4.5486. From Fig. 2, it is observed that the scale-dependent motion of the nanofluid-conveying viscoelastic nanotube is period-1 for this speed. It implies that in the sub-critical regime, when the nanofluid speed is sufficiently smaller than the critical speed, the period-1 motion governs the viscoelastic nanosystem. To further illustrate the period-1 motion of the nanofluid-conveying nanotube (described in Fig. 2), the dynamical characteristics of this scale-dependent motion at F_1=30.0 is plotted in Fig. 3. Three different types of diagrams are shown, namely the Fourier transforms (FFTs), phase-plane portraits and time histories.

Figure 4 depicts the scale-dependent bifurcation response of the Poincaré section of the nanotube conveying nanofluid for a speed close to the critical region in the sub-critical regime (U =4.10<U_{cr}); the transverse motion is shown at x=0.45. The nanosystem natural frequency is determined as ω_1=1.8275. As can be seen from the figure, for this nanofluid speed, various scale-dependent motion types including period-1, period-3 and chaos are observed. At the beginning, the period-1 motion is found for the nanosystem. However, as the force amplitude increases, the viscoelastic nanosystem experiences various motion types. Another important observation is that there are five different chaotic regions in the

nonlinear dynamic response of the viscoelastic nanotube conveying nanofluid flow near the critical region in the sub-critical regime. In addition, Figs. 5 and 6 give more details of the dynamical characteristics of the period-3 motion at F_1=5.0 and the chaotic motion at F_1=28.1, respectively.

In Fig. 7, the bifurcation response of the Poincaré section of the nanotube conveying nanofluid is plotted for a speed a little higher than the critical value (U=4.16>U_{cr}). The transverse motion is plotted at x=0.45. The natural frequency of the nanofluid-conveying nanotube is ω_1= 2.4584. Again, various scale-dependent motions including period-i (i=1,2,3) and chaos are seen for the nanosystem. Comparing Figs. 4 and 7, it is found that a slight change in the nanofluid speed near the critical value can significantly alter the nonlinear scale-dependent motion of the viscoelastic nanotube; particularly, a slight rise in the nanofluid speed shifts the regions in which chaotic motions occur. For more details, the dynamical characteristics of the chaotic motion at F_1=5.4, the periodic motion at F_1=25.0 and the chaotic motion at F_1=40.5 are shown in Figs. 8, 9 and 10, respectively.

Figure 11 illustrates the bifurcation response of the Poincaré section of the nanotube conveying nanofluid for a nanofluid speed higher than the critical value (U=4.30>U_{cr}). The transverse defection of the viscoelastic nanotube is obtained at x=0.45. A value of ω_1= 5.8445 is determined for the natural frequency of the nanosystem. It is found that at the beginning, the nonlinear dynamic response of the nanosystem is period-1. As the force amplitude further increases, other motion types including period-3 and chaos are observed in the nonlinear dynamic response of the nanotube conveying nanofluid flow. However,

compared to Fig. 7 (U = 4.16), less motion complexity is observed in Fig. 11 (U=4.30) for the viscoelastic nanosystem. This implies that in the super-critical regime, a slight rise in the nanofluid speed noticeably reduces the motion complexity of the viscoelastic nanotube. The motion dynamical characteristics at F_1=3.4 for the system of Fig. 11 are demonstrated in Fig. 12. Furthermore, the motion dynamical characteristics at F_1=40.0 for the system of Fig. 11 are illustrated in Fig. 13. It is concluded that at F_1=3.4, the nanosystem motion is of chaotic type while at F_1=40.0, it exhibits a period-3 motion.

From full diagrams, it can be concluded that depending on the fluid velocity, chaos in the motion of the viscoelastic nanotube conveying nanofluid flow can be reduced or increased. The chance of occurring chaos in the fluid-conveying nanotube rapidly grows by increasing the fluid velocity in the subcritical regime near the critical point. Nonetheless, in the supercritical regime, increasing the fluid velocity reduces chaos in the nanosystem. This is due to the fact that increasing the fluid velocity in the subcritical regime (or decreasing the velocity in the supercritical one), the fluid-conveying nanosystem approaches the critical point corresponding to buckling.

Figure 14 is plotted to study the small-scale effects on the subcritical and supercritical fundamental natural frequencies of the nanotube conveying nanofluid flow. The nonlocal parameter has a decreasing influence on the total stiffness of nanostructures while the strain gradient parameter has an increasing influence. This implies that the critical velocity corresponding to buckling decreases with increasing e_0a while increasing l_{sg} increases the critical fluid velocity, as seen in the figure.

4. Conclusions

A nonlinear scale-dependent fluid-structure interaction model was developed for the chaotic motion of viscoelastic nanotubes conveying nanofluid flow. The viscoelastic nanosystem was subject to an external excitation in the transverse direction. Size effects were incorporated in both solid and fluid parts of the viscoelastic nanosystem. Moreover, the effects of both centripetal and Coriolis accelerations were taken into account. Employing the Beskok-Karniadaki theory, nonlocal strain gradient elasticity and Hamilton's principle, the nonlinear scale-dependent equation was derived. A precise solution approach on the basis of Galerkin's procedure and a direct-time-integration method was presented for the nonlinear scale-dependent equation of the nanotube conveying nanofluid.

It was concluded that the viscoelastic nanotube conveying nanofluid flow exhibits the period-1 motion when the nanofluid speed is adequately smaller than the critical speed. However, when the nanofluid speed approaches the critical value in the sub-critical regime, various scale-dependent motions including period-i (i=1,3) and chaos are seen in the nonlinear dynamic behaviour. Moreover, it was found that near the critical speed, a slight change in the value of the nanofluid speed can noticeably alter the nonlinear motion of the viscoelastic nanosystem. It was also observed that when the nanofluid speed is higher than the critical value, the motion type of the nanotube conveying nanofluid flow is period-1 for small force amplitudes. Nonetheless, other motion types including period-3 and chaos are observed with increasing force amplitude. Furthermore, depending on system parameters, in the super-critical regime, the complexity of the motion of the viscoelastic nanotube conveying nanofluid flow can be reduced by increasing nanofluid speed.

Appendix A: a convergence study

A convergence test is performed in order to indicate that eight eigenfunctions are enough to obtain a precise solution. Figure 15 shows the bifurcation diagrams of Poincaré sections of the nanotube conveying nanofluid flow for different degrees of freedom. The dimensionless fluid velocity is set to U=4.10. It is found that two and four degrees of freedom are not enough to obtain an accurate solution while eight degrees of freedom lead to a converged solution.

Appendix B: a verification study

For verification purposes, a linear nanoscale tube conveying nanofluid flow is taken into consideration. Using Eq. (25) and neglecting geometrical nonlinearity, one obtains

$$\begin{aligned} &EI\left(1-l_{sg}^2\nabla^2\right)\left(1+\tau_d\frac{\partial}{\partial t}\right)\frac{\partial^4 w}{\partial x^4} \\ &+\left(m_{nt}+m_{nf}\right)\frac{\partial^2 w}{\partial t^2}+2m_{nf}U\frac{\partial^2 w}{\partial t\partial x}+m_{nf}U^2\frac{\partial^2 w}{\partial x^2} \\ &-\left(e_0 a\right)^2\nabla^2\left[\left(m_{nt}+m_{nf}\right)\frac{\partial^2 w}{\partial t^2}+2m_{nf}U\frac{\partial^2 w}{\partial t\partial x}+m_{nf}U^2\frac{\partial^2 w}{\partial x^2}\right]=0, \end{aligned} \tag{B1}$$

in which $\tau_d=\eta/E$. It should be noticed that the effects of the speed correction factor are also ignored in the above equation. For the transverse displacement, one can write

$$w=We^{(ikx-i\omega t)}, \tag{B2}$$

where k and ω are the wave number and frequency of the nanotube, respectively. Substituting Eq. (B2) into Eq. (B1) yields the following relation

$$\left(1+\left(e_0a\right)^2k^2\right)\left(m_{nt}+m_{nf}\right)\omega^2$$
$$-\left[2m_{nf}Uk\left(1+\left(e_0a\right)^2k^2\right)-i\tau_dEI\left(1+l_{sg}^2k^2\right)k^4\right]\omega \tag{B3}$$
$$-EI\left(1+l_{sg}^2k^2\right)k^4+m_{nf}U^2k^2\left(1+\left(e_0a\right)^2k^2\right)=0,$$

The above equation for the linear frequency of nanotubes conveying nanofluid flow is the same as that obtained in the literature (Li and Hu, 2016).

References

Arani, A., Haghparast, E., Arani, A., 2016. Size-dependent vibration of double-bonded carbon nanotube-reinforced composite microtubes conveying fluid under longitudinal magnetic field. Polymer Composites 37, 1375-1383.

Arani, A.G., Bagheri, M., Kolahchi, R., Maraghi, Z.K., 2013a. Nonlinear vibration and instability of fluid-conveying DWBNNT embedded in a visco-Pasternak medium using modified couple stress theory. Journal of Mechanical Science and Technology 27, 2645-2658.

Arani, A.G., Dashti, P., Amir, S., Yousefi, M., 2015. Flexural vibration of coupled double-walled Carbon nanotubes conveying fluid under thermo-magnetic fields based on strain gradient theory. Journal of Theoretical and Applied Mechanics 53, 947-957.

Arani, A.G., Hashemian, M., Kolahchi, R., 2013b. Time discretization effect on the nonlinear vibration of embedded SWBNNT conveying viscous fluid. Composites Part B: Engineering 54, 298-306.

Arani, A.G., Mortazavi, S.A., Maraghi, Z.K., 2017. Dynamic stability of nanocomposite viscoelastic cylindrical shells coating with a piezomagnetic layer conveying pulsating fluid flow. Science and Engineering of Composite Materials 24, 401-414.

Ashoori Movassagh, A., Mahmoodi, M.J., 2013. A micro-scale modeling of Kirchhoff plate based on modified strain-gradient elasticity theory. European Journal of Mechanics - A/Solids 40, 50-59.

Aydogdu, M., 2014. Longitudinal wave propagation in multiwalled carbon nanotubes. Composite Structures 107, 578-584.

Bahaadini, R., Saidi, A.R., 2018. Stability analysis of thin-walled spinning reinforced pipes conveying fluid in thermal environment. European Journal of Mechanics, A/Solids 72, 298-309.

Beskok, A., Karniadakis, G.E., 1999. Report: a model for flows in channels, pipes, and ducts at micro and nano scales. Microscale Thermophysical Engineering 3, 43-77.

Deng, J., Liu, Y., Zhang, Z., Liu, W., 2017. Stability analysis of multi-span viscoelastic functionally graded material pipes conveying fluid using a hybrid method. European Journal of Mechanics, A/Solids 65, 257-270.

Farajpour, A., Ghayesh, M.H., Farokhi, H., 2018a. A review on the mechanics of nanostructures. International Journal of Engineering Science 133, 231-263.

Farajpour, M., Shahidi, A., Tabataba'i-Nasab, F., Farajpour, A., 2018b. Vibration of initially stressed carbon nanotubes under magneto-thermal environment for nanoparticle delivery via higher-order nonlocal strain gradient theory. The European Physical Journal Plus 133, 219.

Filiz, S., Aydogdu, M., 2015. Wave propagation analysis of embedded (coupled) functionally graded nanotubes conveying fluid. Composite Structures 132, 1260-1273.

Ghayesh, M.H., 2018a. Dynamics of functionally graded viscoelastic microbeams. International Journal of Engineering Science 124, 115-131.
Ghayesh, M.H., 2018b. Functionally graded microbeams: Simultaneous presence of imperfection and viscoelasticity. International Journal of Mechanical Sciences 140, 339-350.
Ghayesh, M.H., 2018c. Nonlinear vibration analysis of axially functionally graded shear-deformable tapered beams. Applied Mathematical Modelling 59, 583-596.
Ghayesh, M.H., Amabili, M., Farokhi, H., 2013a. Three-dimensional nonlinear size-dependent behaviour of Timoshenko microbeams. International Journal of Engineering Science 71, 1-14.
Ghayesh, M.H., Farokhi, H., Alici, G., 2016. Size-dependent performance of microgyroscopes. International Journal of Engineering Science 100, 99-111.
Ghayesh, M.H., Farokhi, H., Amabili, M., 2013b. Nonlinear dynamics of a microscale beam based on the modified couple stress theory. Composites Part B: Engineering 50, 318-324.
Ghayesh, M.H., Farokhi, H., Amabili, M., 2014. In-plane and out-of-plane motion characteristics of microbeams with modal interactions. Composites Part B: Engineering 60, 423-439.
Ghayesh, M.H., Païdoussis, M.P., Modarres-Sadeghi, Y., 2011. Three-dimensional dynamics of a fluid-conveying cantilevered pipe fitted with an additional spring-support and an end-mass. Journal of Sound and Vibration 330, 2869-2899.
Gholipour, A., Farokhi, H., Ghayesh, M.H., 2015. In-plane and out-of-plane nonlinear size-dependent dynamics of microplates. Nonlinear Dynamics 79, 1771-1785.
Hosseini, M., Sadeghi-Goughari, M., 2016. Vibration and instability analysis of nanotubes conveying fluid subjected to a longitudinal magnetic field. Applied Mathematical Modelling 40, 2560-2576.
Lee, H.-L., Chang, W.-J., 2009. Vibration analysis of a viscous-fluid-conveying single-walled carbon nanotube embedded in an elastic medium. Physica E: Low-dimensional Systems and Nanostructures 41, 529-532.
Li, L., Hu, Y., 2015. Buckling analysis of size-dependent nonlinear beams based on a nonlocal strain gradient theory. International Journal of Engineering Science 97, 84-94.
Li, L., Hu, Y., 2016. Wave propagation in fluid-conveying viscoelastic carbon nanotubes based on nonlocal strain gradient theory. Computational materials science 112, 282-288.
Li, L., Hu, Y., Li, X., Ling, L., 2016. Size-dependent effects on critical flow velocity of fluid-conveying microtubes via nonlocal strain gradient theory. Microfluidics and Nanofluidics 20, 76.
Lim, C., Zhang, G., Reddy, J., 2015. A higher-order nonlocal elasticity and strain gradient theory and its applications in wave propagation. Journal of the Mechanics and Physics of Solids 78, 298-313.
Liu, M., Wang, Z., Zhou, Z., Qu, Y., Yu, Z., Wei, Q., Lu, L., 2018. Vibration response of multi-span fluid-conveying pipe with multiple accessories under complex boundary conditions. European Journal of Mechanics, A/Solids 72, 41-56.
Ma, H., Gao, X.-L., Reddy, J., 2008. A microstructure-dependent Timoshenko beam model based on a modified couple stress theory. Journal of the Mechanics and Physics of Solids 56, 3379-3391.
Rafiei, M., Mohebpour, S.R., Daneshmand, F., 2012. Small-scale effect on the vibration of non-uniform carbon nanotubes conveying fluid and embedded in viscoelastic medium. Physica E: Low-Dimensional Systems and Nanostructures 44, 1372-1379.
Rashidi, V., Mirdamadi, H.R., Shirani, E., 2012. A novel model for vibrations of nanotubes conveying nanoflow. Computational Materials Science 51, 347-352.
Reddy, J., Pang, S., 2008. Nonlocal continuum theories of beams for the analysis of carbon nanotubes. Journal of Applied Physics 103, 023511.
Saadatnia, Z., Esmailzadeh, E., 2017. Nonlinear harmonic vibration analysis of fluid-conveying piezoelectric-layered nanotubes. Composites Part B: Engineering 123, 193-209.

Şimşek, M., Reddy, J., 2013. Bending and vibration of functionally graded microbeams using a new higher order beam theory and the modified couple stress theory. International Journal of Engineering Science 64, 37-53.
Sinir, B.G., Demir, D.D., 2015. The analysis of nonlinear vibrations of a pipe conveying an ideal fluid. European Journal of Mechanics, B/Fluids 52, 38-44.
Sudak, L., 2003. Column buckling of multiwalled carbon nanotubes using nonlocal continuum mechanics. Journal of applied physics 94, 7281-7287.
Wang, B., Zhou, S., Zhao, J., Chen, X., 2011. A size-dependent Kirchhoff micro-plate model based on strain gradient elasticity theory. European Journal of Mechanics - A/Solids 30, 517-524.
Wang, L., 2009. Vibration and instability analysis of tubular nano-and micro-beams conveying fluid using nonlocal elastic theory. Physica E: Low-dimensional Systems and Nanostructures 41, 1835-1840.
Xia, W., Wang, L., 2010. Vibration characteristics of fluid-conveying carbon nanotubes with curved longitudinal shape. Computational Materials Science 49, 99-103.
Yoon, J., Ru, C., Mioduchowski, A., 2005. Vibration and instability of carbon nanotubes conveying fluid. Composites Science and Technology 65, 1326-1336.
Zhang, B., He, Y., Liu, D., Gan, Z., Shen, L., 2013. A non-classical Mindlin plate finite element based on a modified couple stress theory. European Journal of Mechanics - A/Solids 42, 63-80.
Zhang, J., Meguid, S., 2016. Effect of surface energy on the dynamic response and instability of fluid-conveying nanobeams. European Journal of Mechanics-A/Solids 58, 1-9.
Zhen, Y.-X., Fang, B., 2015. Nonlinear vibration of fluid-conveying single-walled carbon nanotubes under harmonic excitation. International Journal of Non-Linear Mechanics 76, 48-55.

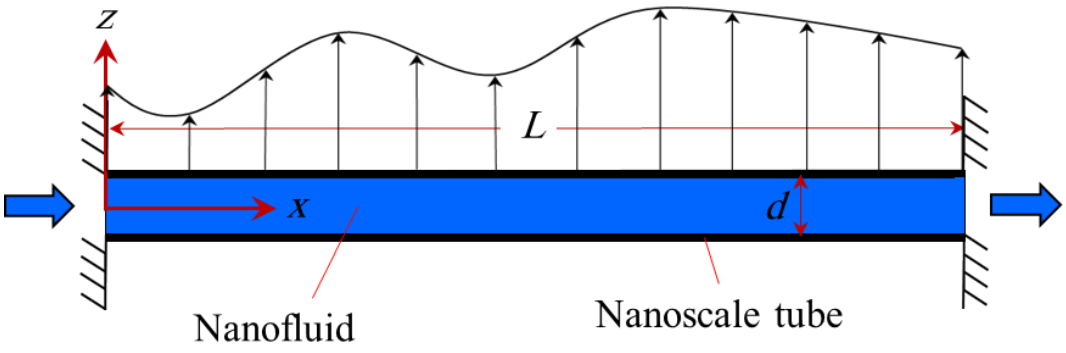

Figure 1. A nanoscale tube conveying fluid flow subject to external loading.

(a)

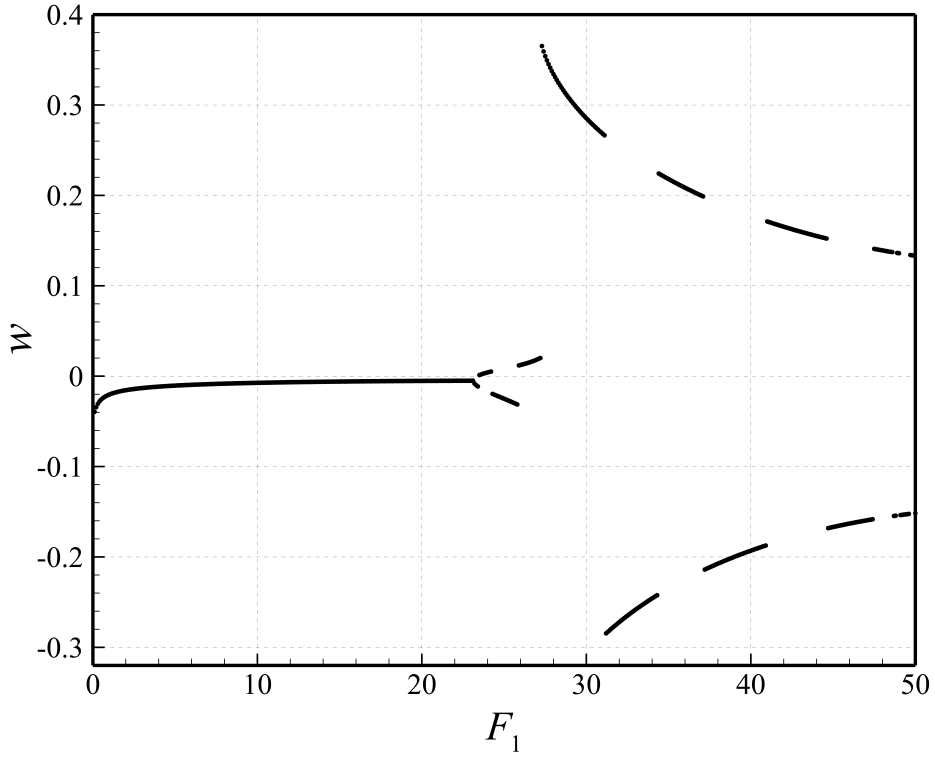
0.4
0.3
0.2
0.1
0
-0.1
-0.2
-0.3
w
0
10
20
30
40
50
F_1

(b)

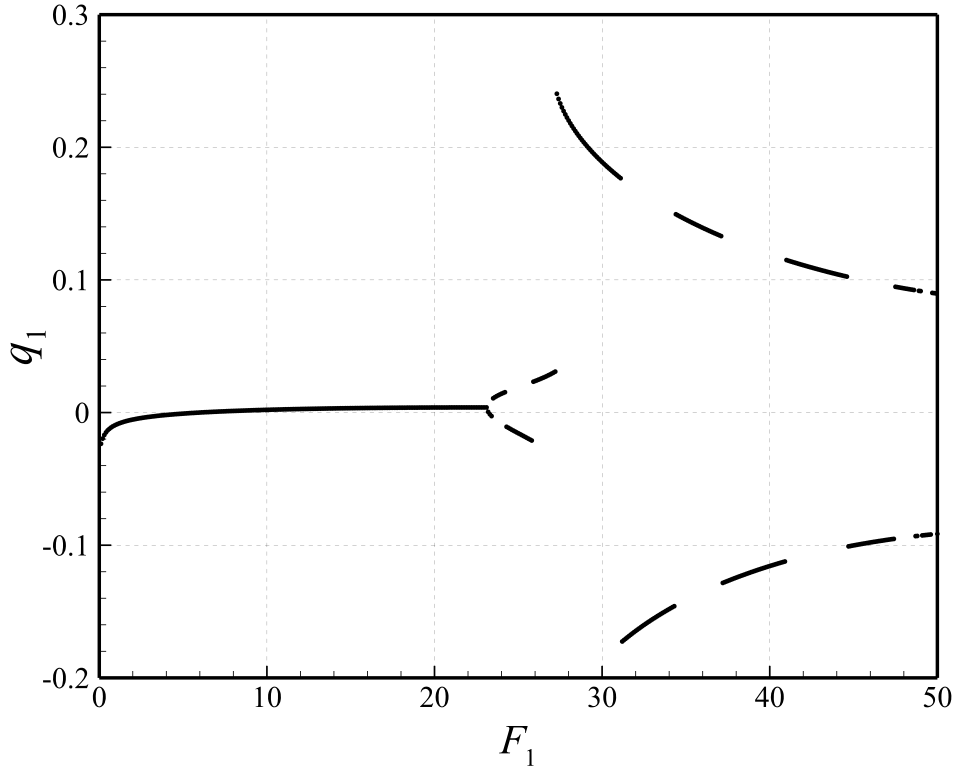
0.3
0.2
0.1
0
-0.1
-0.2
q_1
0
10
20
30
40
50
F_1

(c)

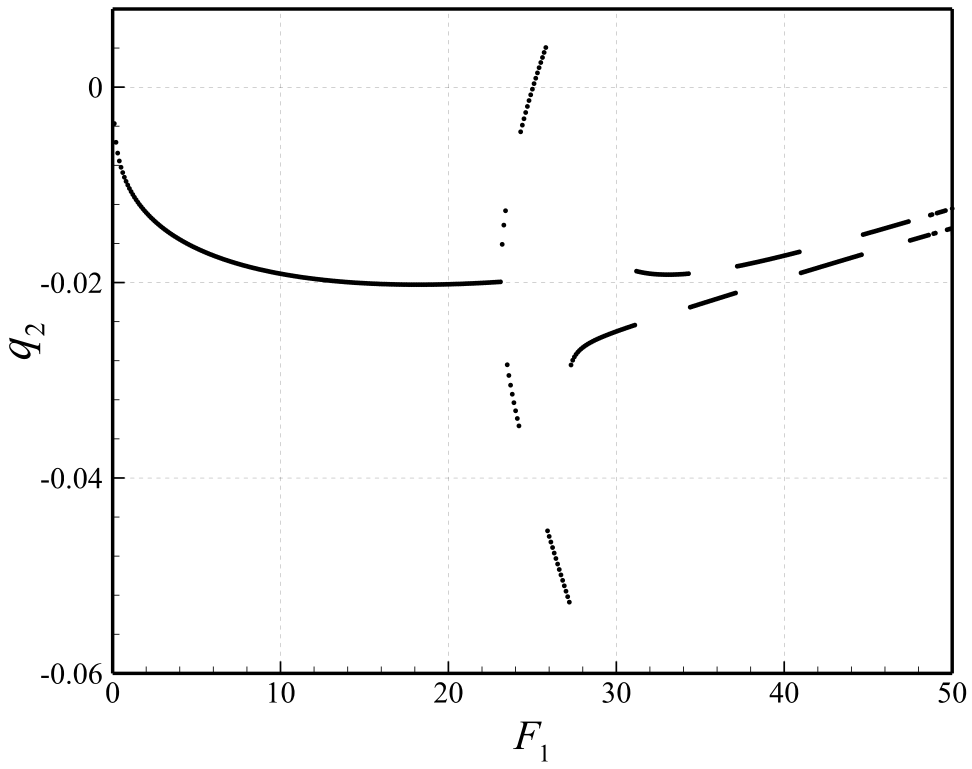

Figure 2: Bifurcation response of the Poincaré section of the nanotube conveying nanofluid for U = 3.95: (a) the transverse motion at x=0.45; (b, c) q_1 and q_2.

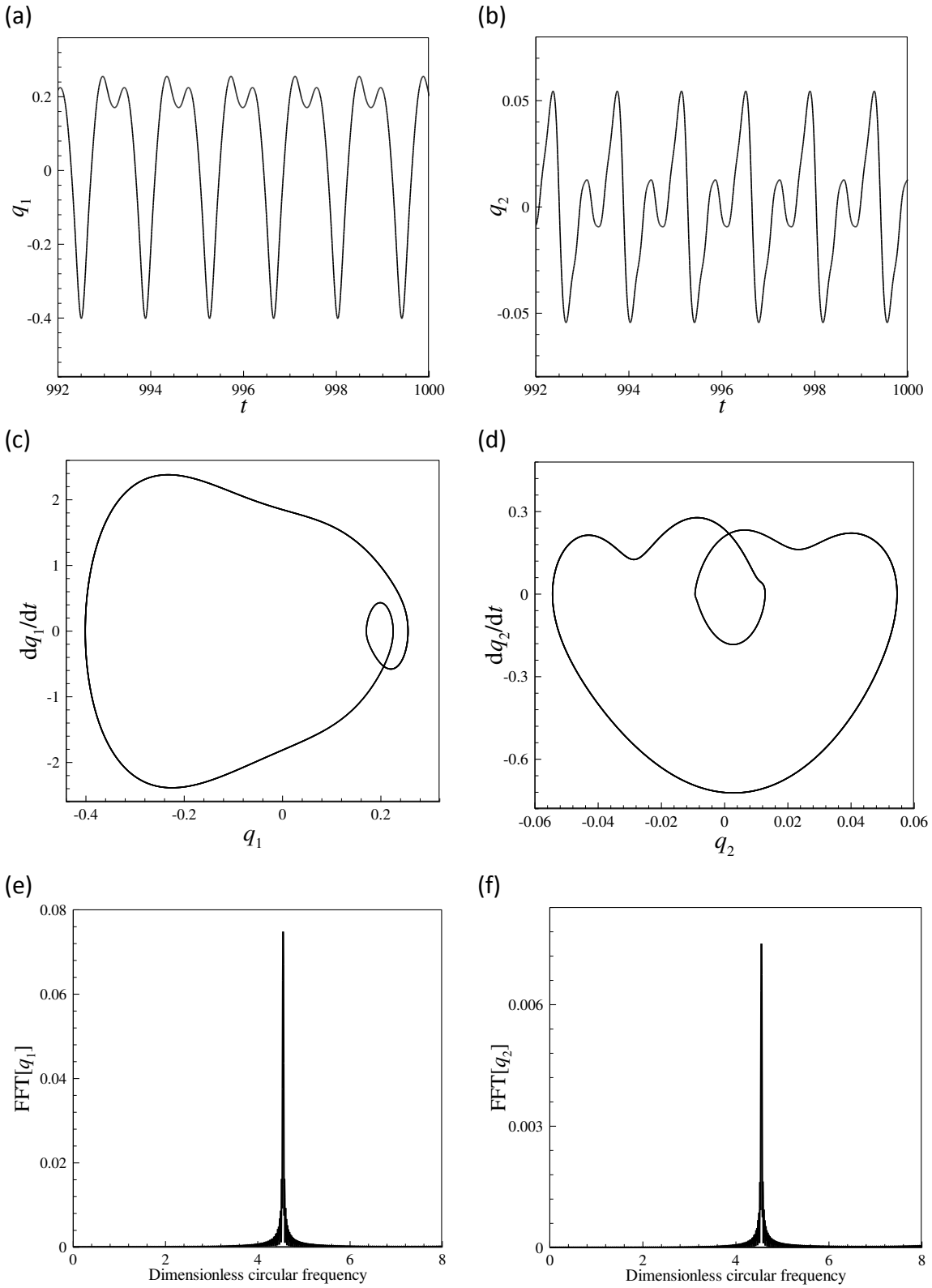

Figure 3: Dynamical characteristics of the system at F_1=30.0 for the periodic motion of Fig. 2: (a) the time history of q_1 (b) the time history of q_2 (c) the phase-plane diagram of q_1 (d) the phase-plane diagram of q_2 (e) FFTs of q_1 (f) FFTs of q_2.

(a)

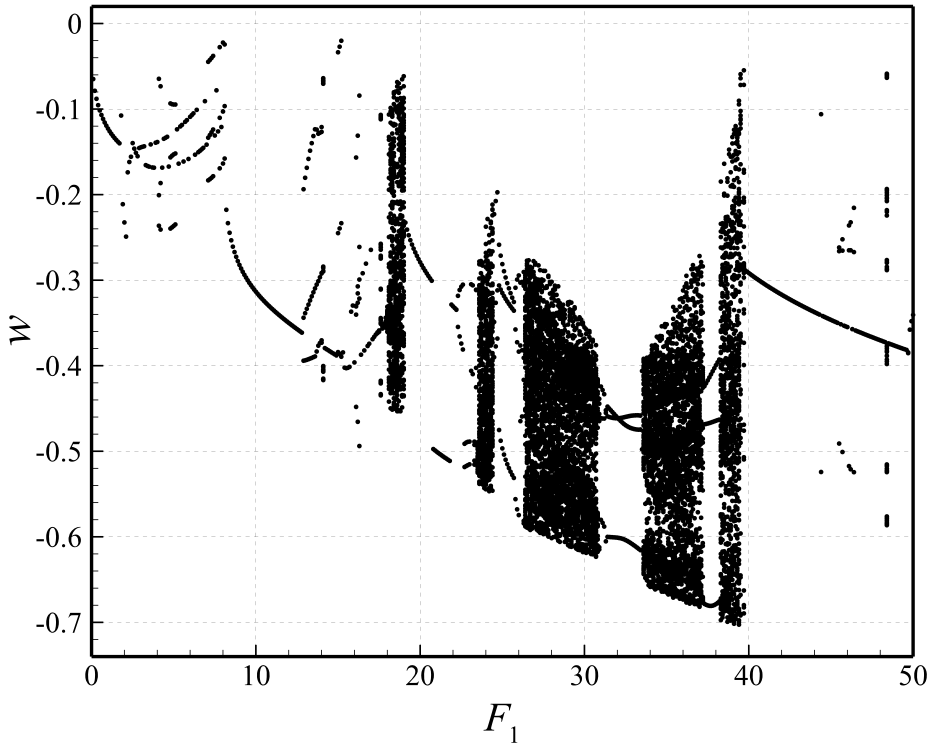
0
-0.1
-0.2
-0.3
-0.4
-0.5
-0.6
-0.7
w
0
10
20
30
40
50
F_1

(b)

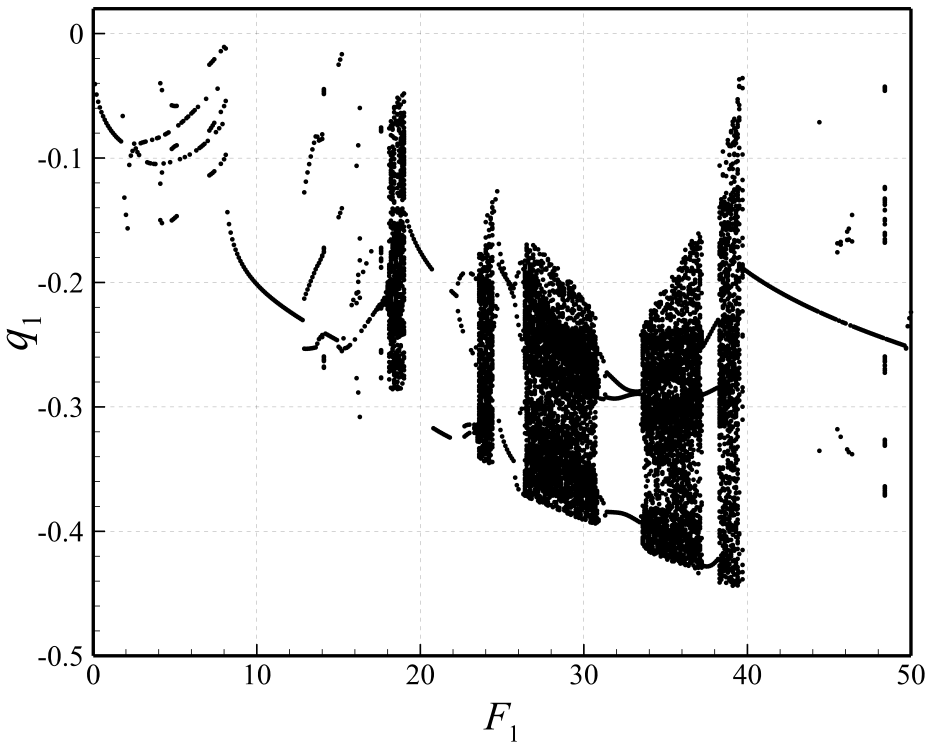
0
-0.1
-0.2
-0.3
-0.4
-0.5
q_1
0
10
20
30
40
50
F_1

(c)

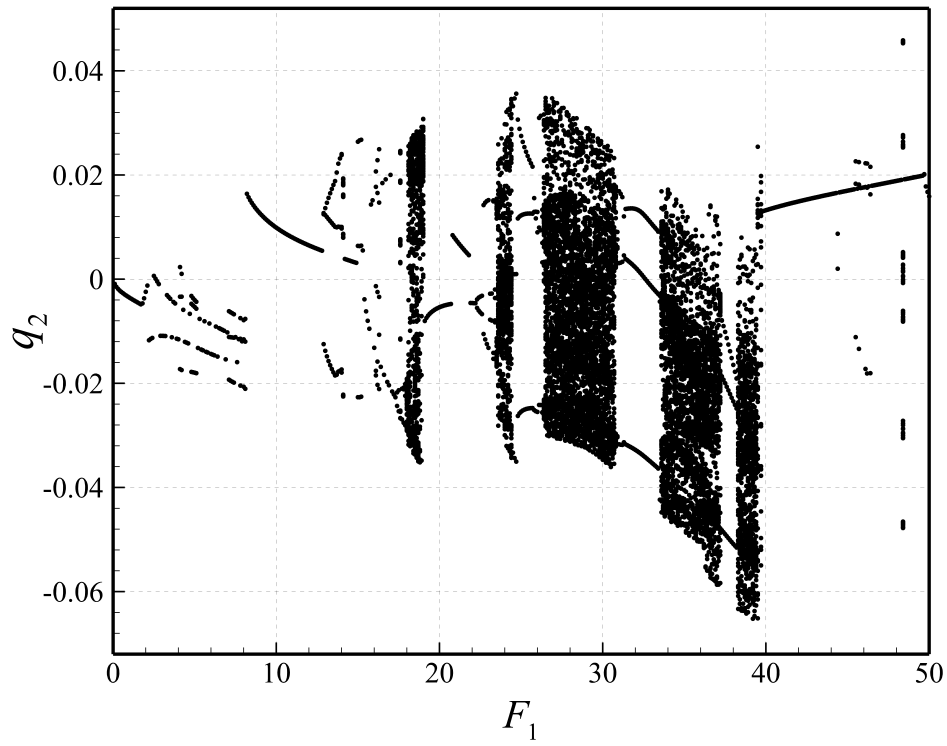

Figure 4: Bifurcation response of the Poincaré section of the nanotube conveying nanofluid for U=4.10 (a) the transverse motion at x=0.45; (b, c) q_1 and q_2.

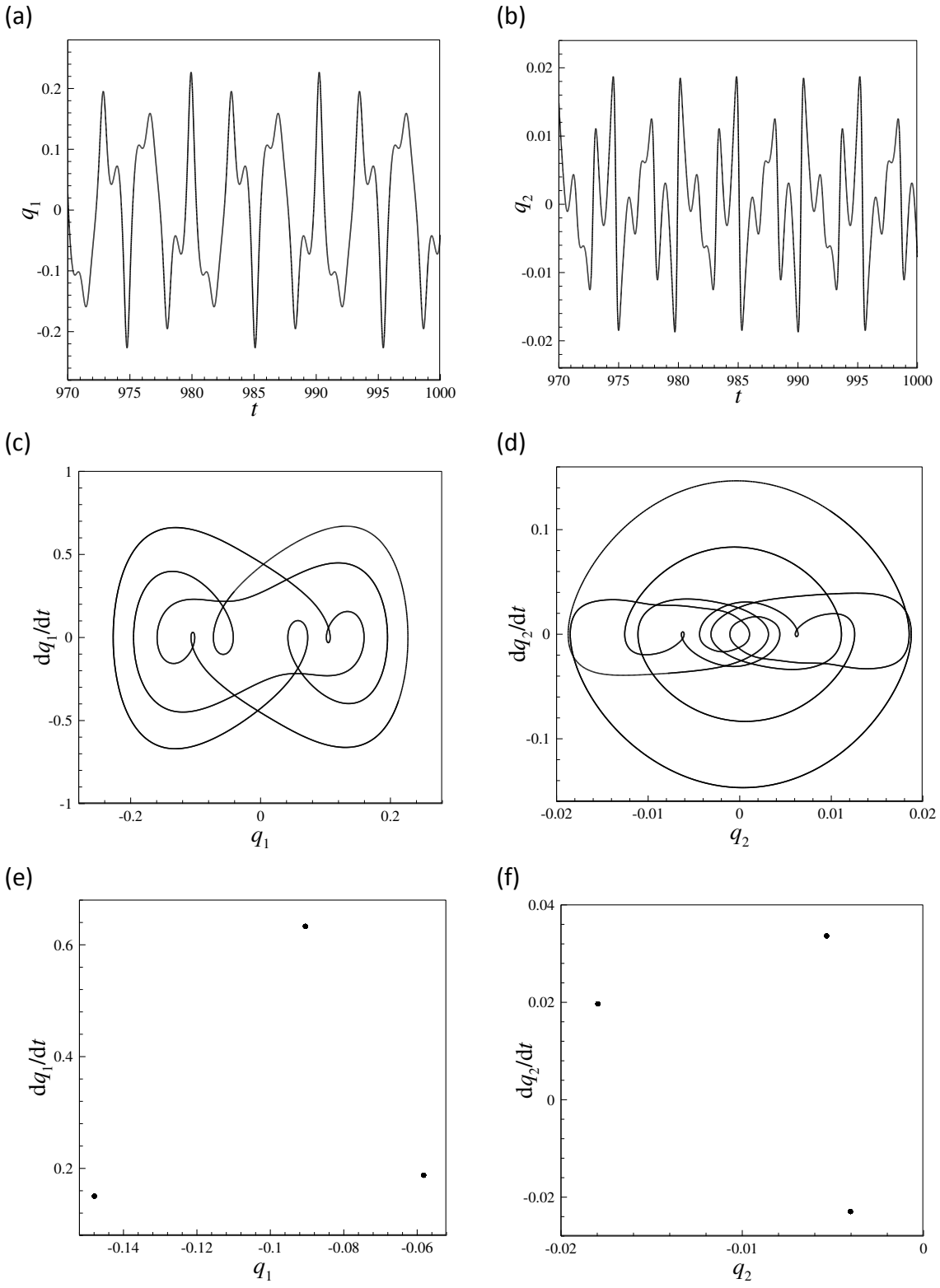

Figure 5: Dynamical characteristics of the system at F_1=5.0 for the period-3 motion of Fig. 4: (a) the time history of q_1 (b) the time history of q_2 (c) the phase-plane diagram of q_1 (d) the phase-plane diagram of q_2 (e) Poincaré sections of q_1 (f) q_2 motions.

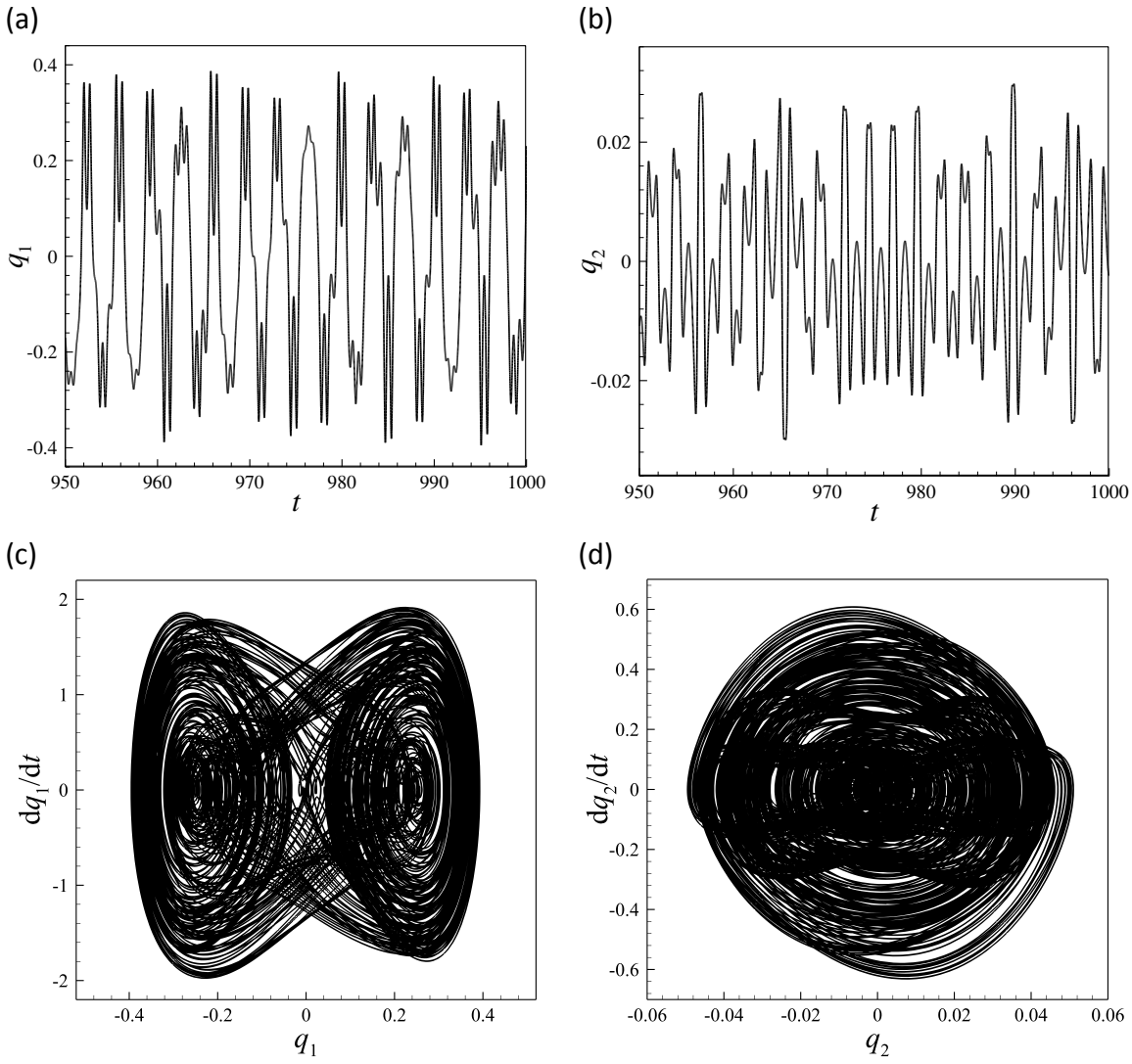

Figure 6: Dynamical characteristics of the system at F_1=28.1 for the chaotic motion of Fig. 4: (a) the time history of q_1 (b) the time history of q_2 (c) the phase-plane diagram of q_1 (d) the phase-plane diagram of q_2.

(a)

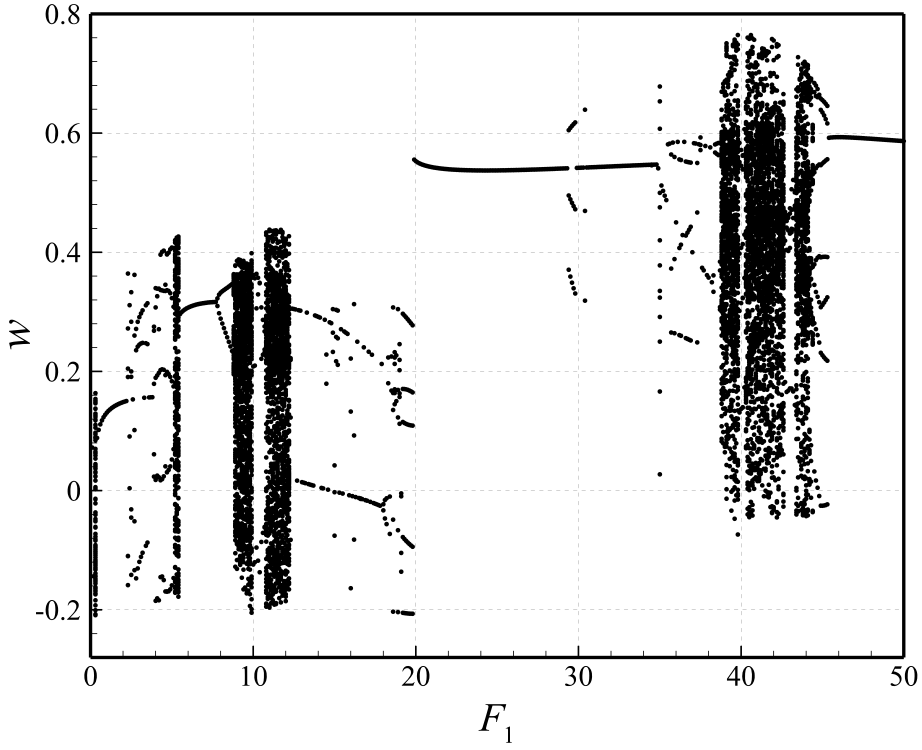
0.8
0.6
0.4
0.2
0
-0.2
w
0
10
20
30
40
50
F_1

(b)

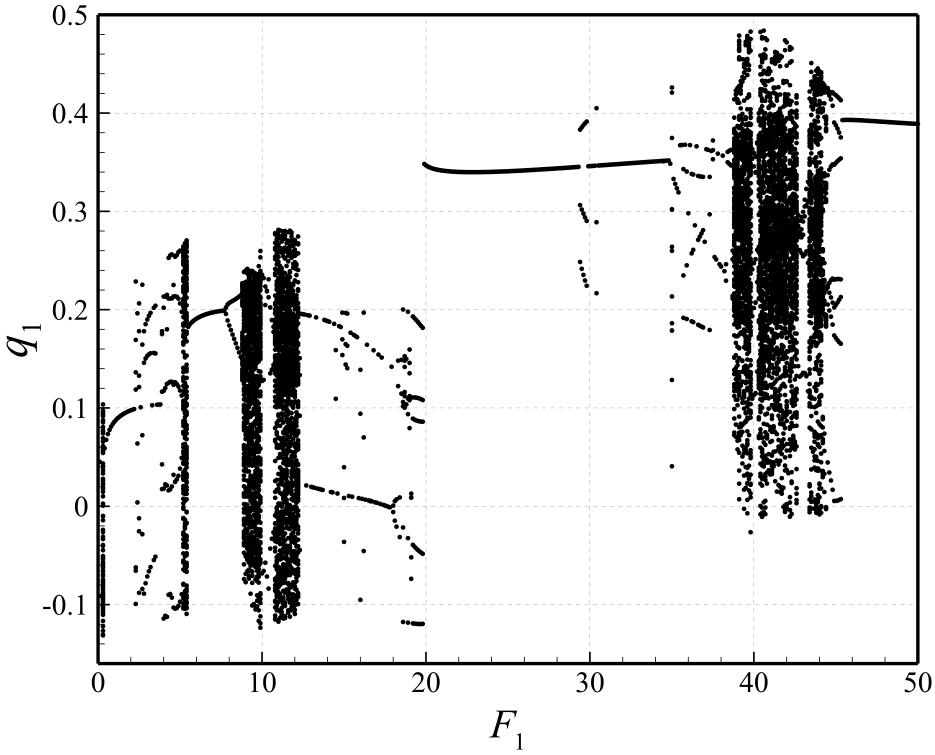
0.5
0.4
0.3
0.2
0.1
0
-0.1
q_1
0
10
20
30
40
50
F_1

(c)

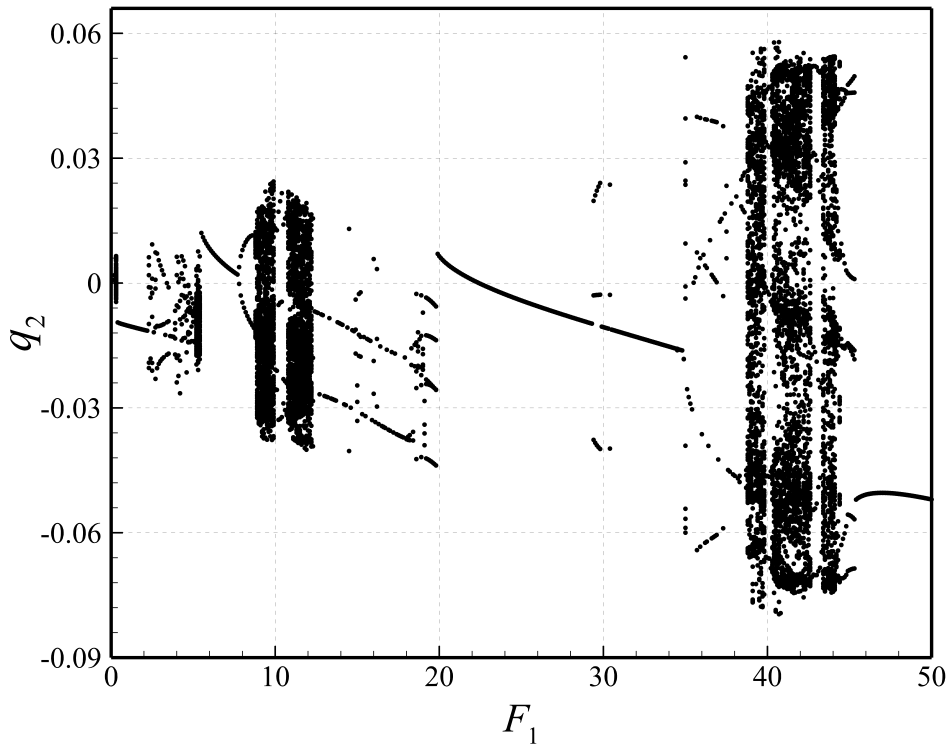

Figure 7: Bifurcation response of the Poincaré section of the nanotube conveying nanofluid for U = 4.16: (a) the transverse motion at x=0.45; (b, c) q_1 and q_2.

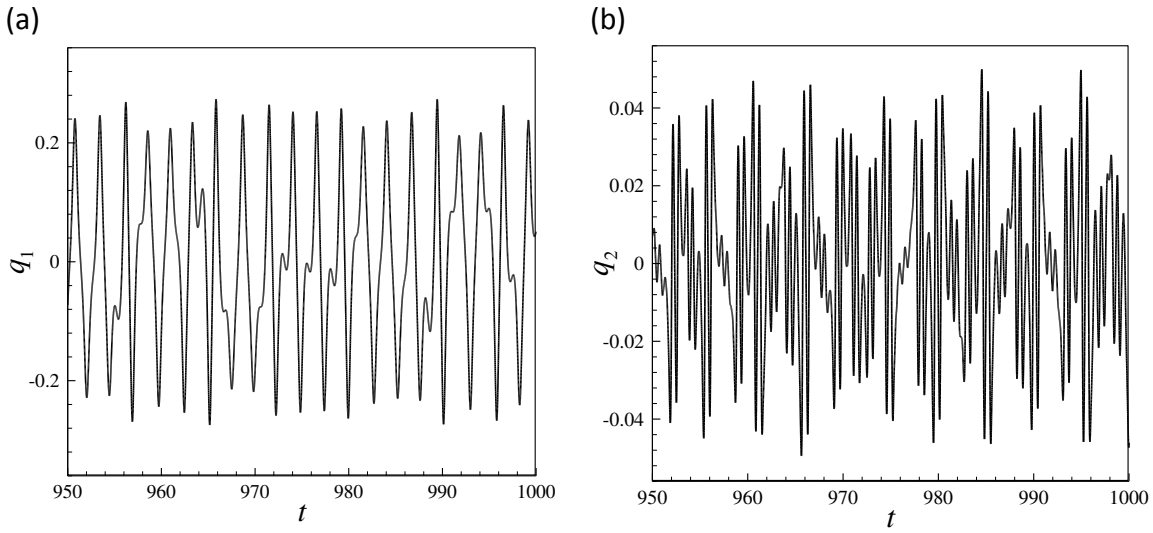

Figure 8: Dynamical characteristics of the system at F_1=5.4 for the chaotic motion of Fig. 7: (a) the time history of q_1 (b) the time history of q_2.

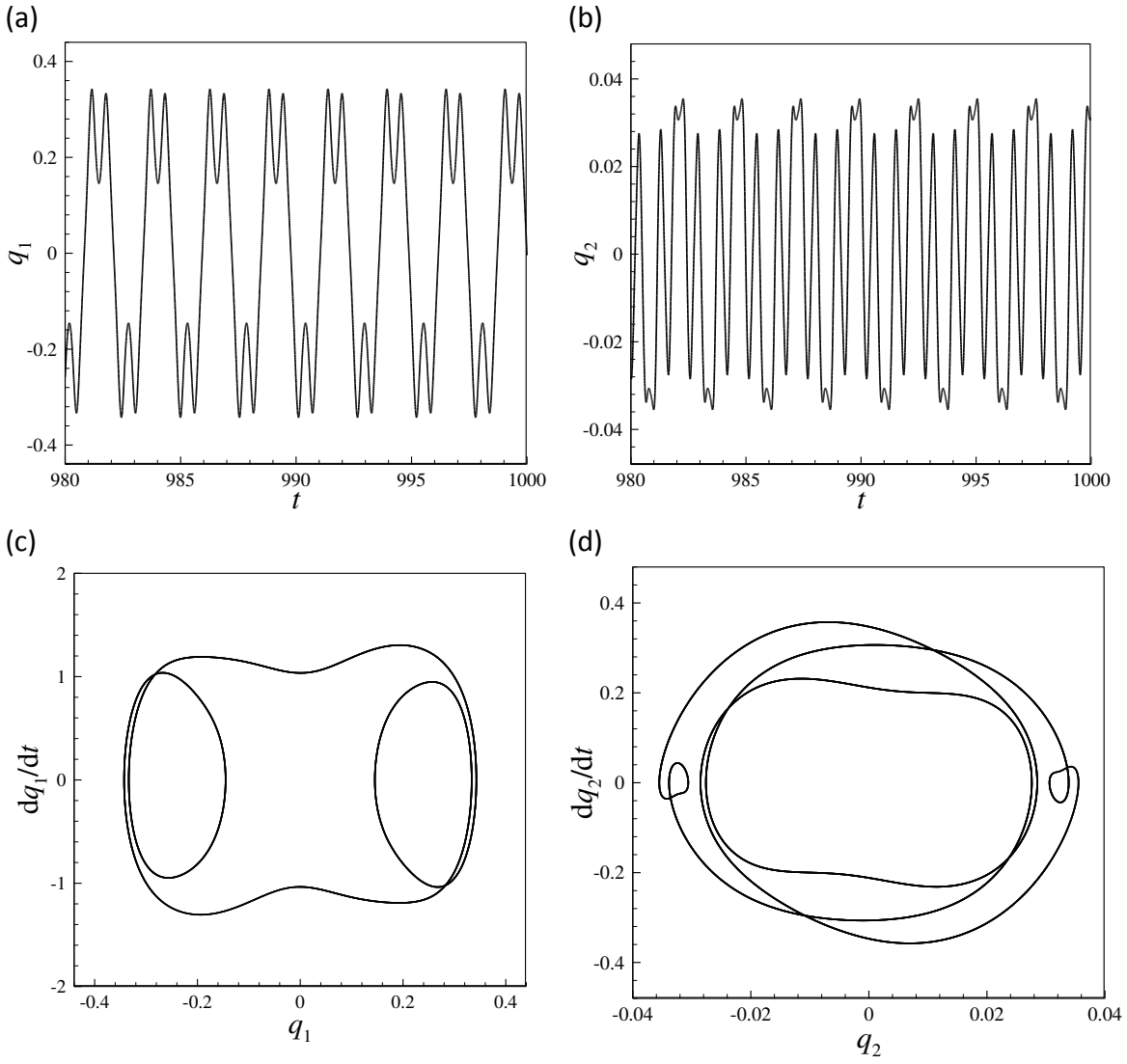

Figure 9: Dynamical characteristics of the system at F_1=25.0 for the periodic motion of Fig. 7: (a) the time history of q_1 (b) the time history of q_2 (c) the phase-plane diagram of q_1 (d) the phase-plane diagram of q_2.

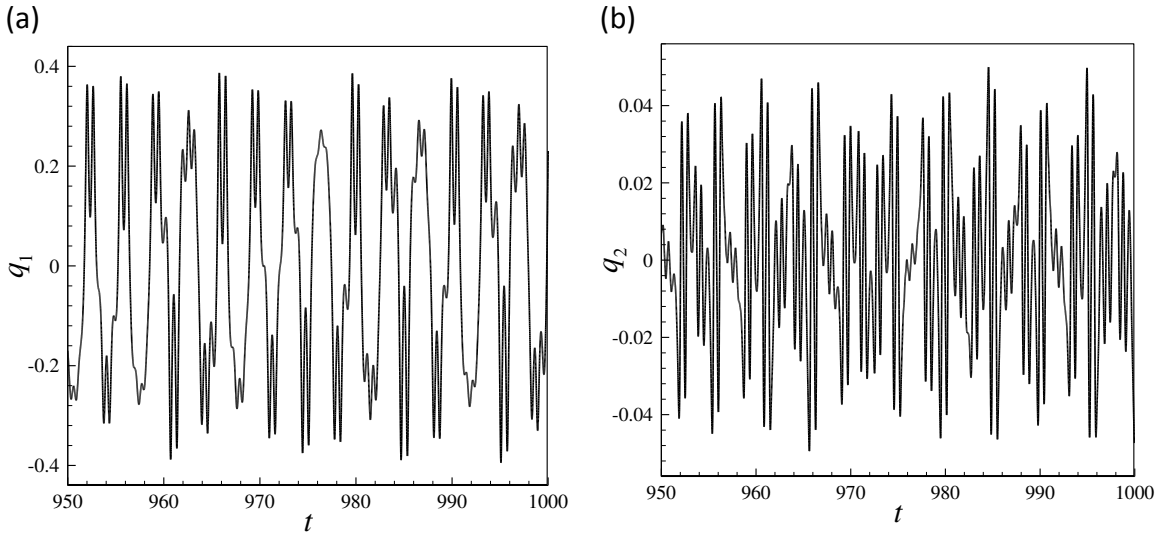

Figure 10: Dynamical characteristics of the system at F_1=40.5 for the chaotic motion of Fig. 7: (a) the time history of q_1 (b) the time history of q_2.

(a)

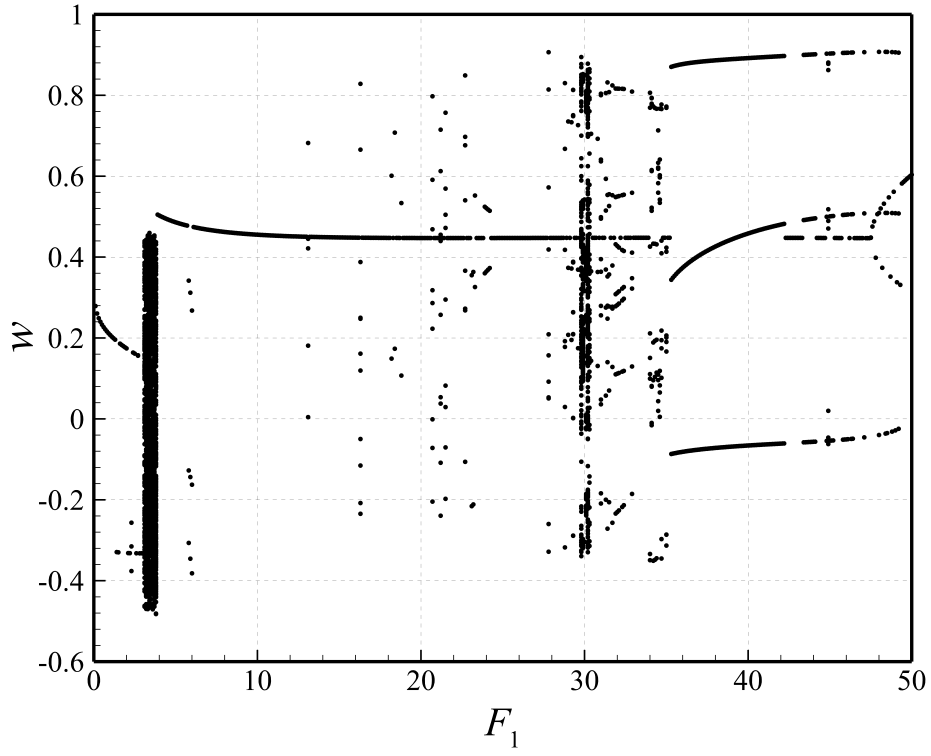
1
0.8
0.6
0.4
0.2
0
-0.2
-0.4
-0.6
w
0
10
20
30
40
50
F_1

(b)

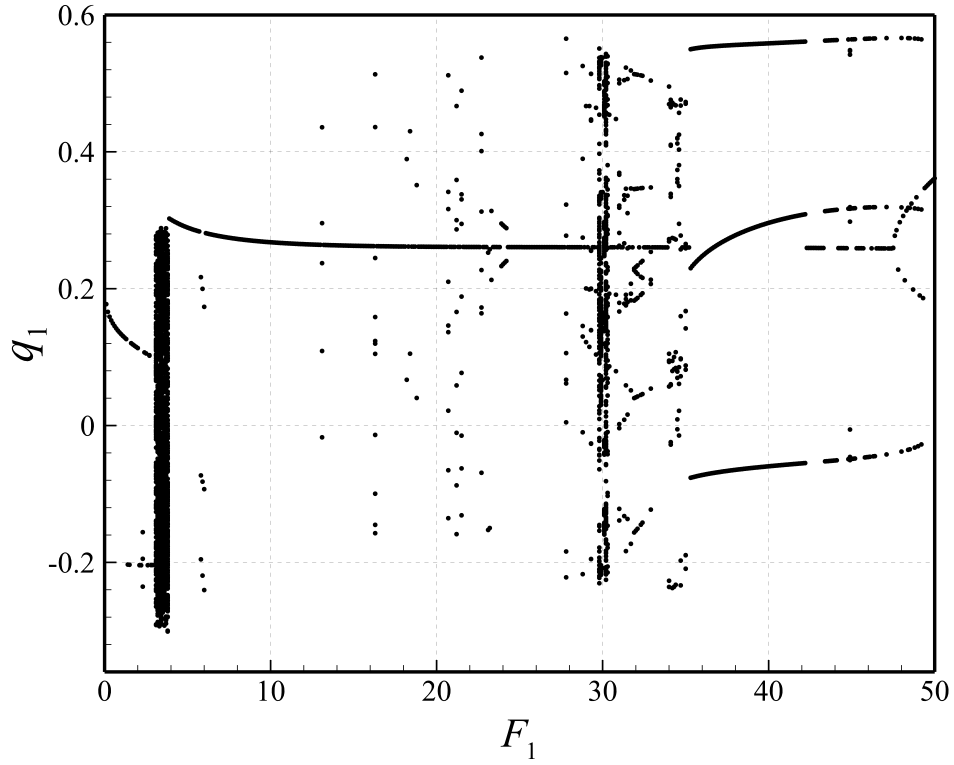
0.6
0.4
0.2
0
-0.2
q_1
0
10
20
30
40
50
F_1

(c)

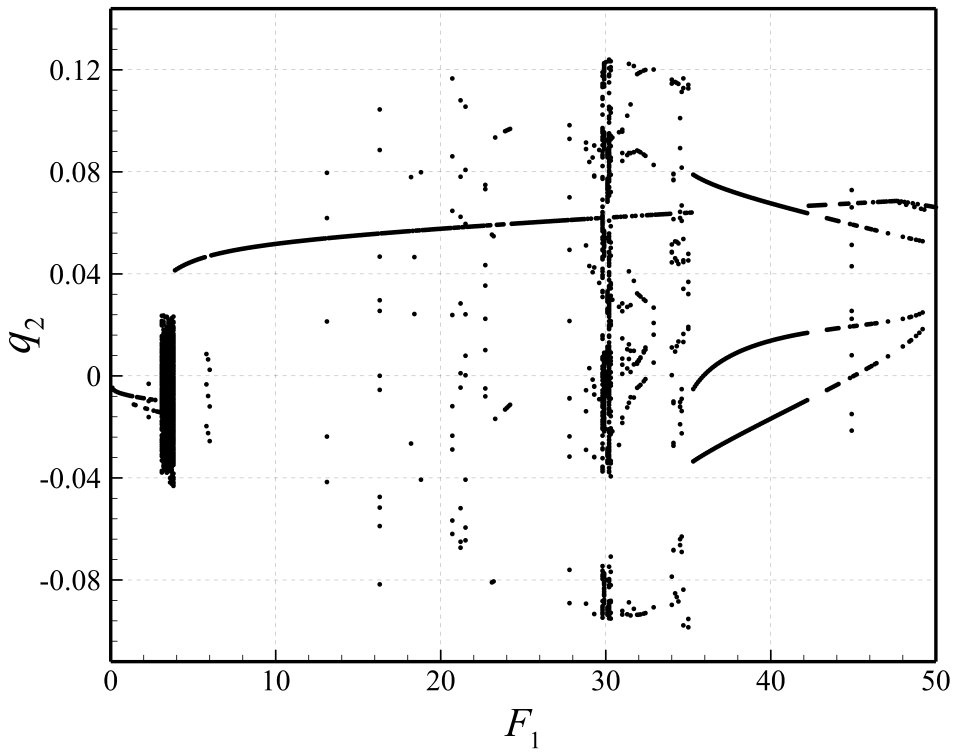

Figure 11: Bifurcation response of the Poincaré section of the nanotube conveying nanofluid for $U = 4.30$: (a) the transverse motion at x=0.45; (b, c) q_1 and q_2.

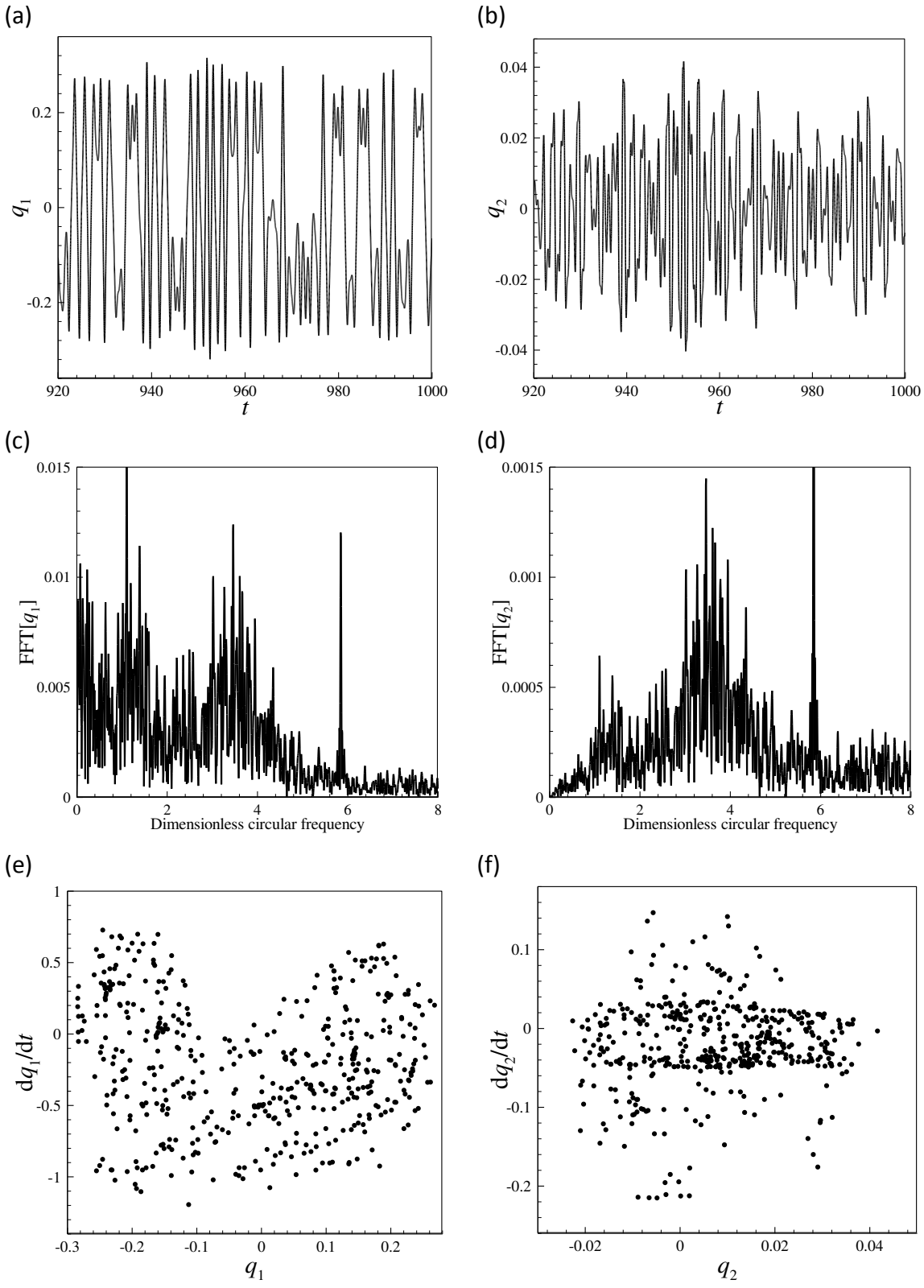

Figure 12: Dynamical characteristics of the system at F_1=3.4 for the chaotic motion of Fig. 11: (a) the time history of q_1 (b) the time history of q_2 (c) FFTs of q_1 (d) FFTs of q_2 (e) Poincaré sections of q_1 (f) q_2 motions.

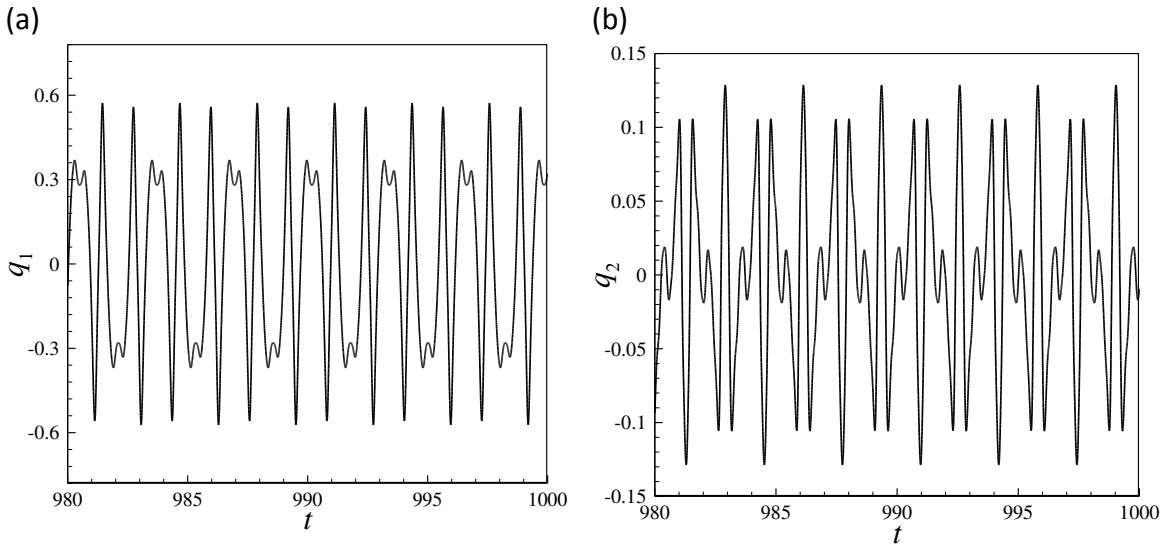

Figure 13: Dynamical characteristics of the system at F_1=40.0 for the period-3 motion of Fig. 11: (a) the time history of q_1 (b) the time history of q_2.

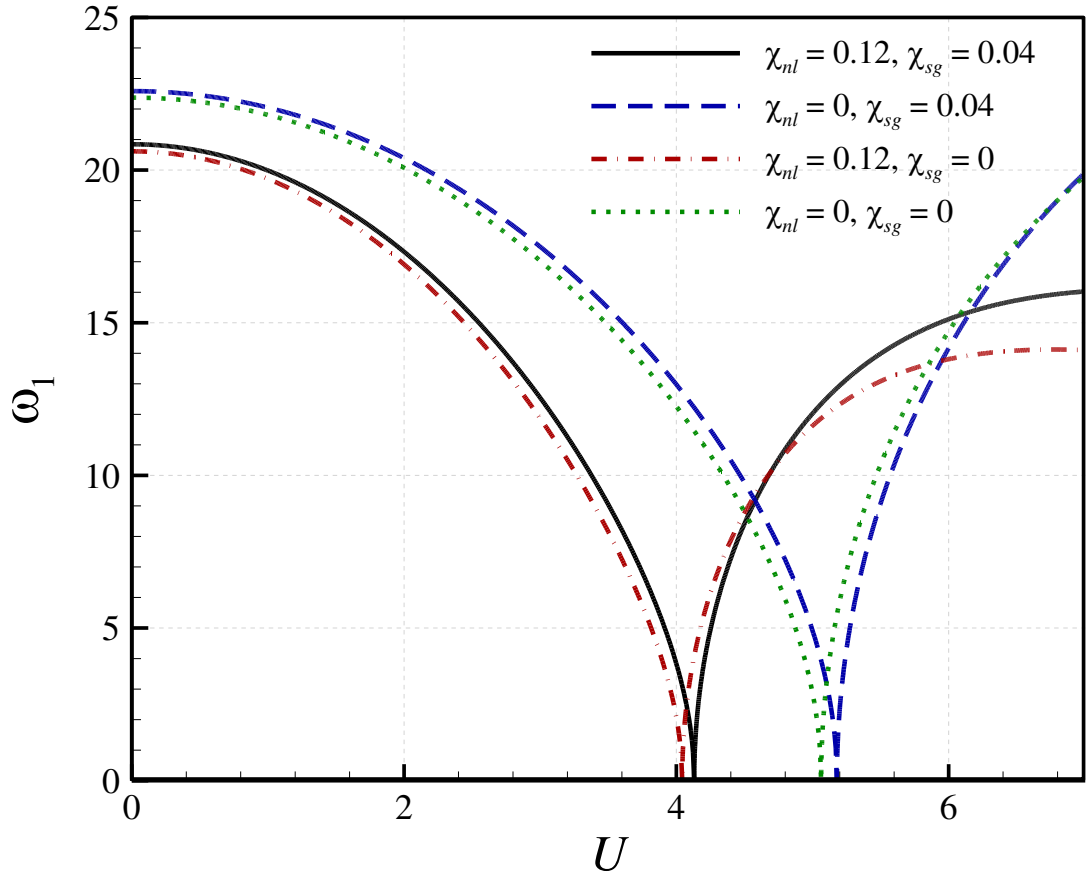

Figure 14: Small-scale effects on the subcritical and supercritical fundamental natural frequencies of the nanotube conveying nanofluid flow.

(a)

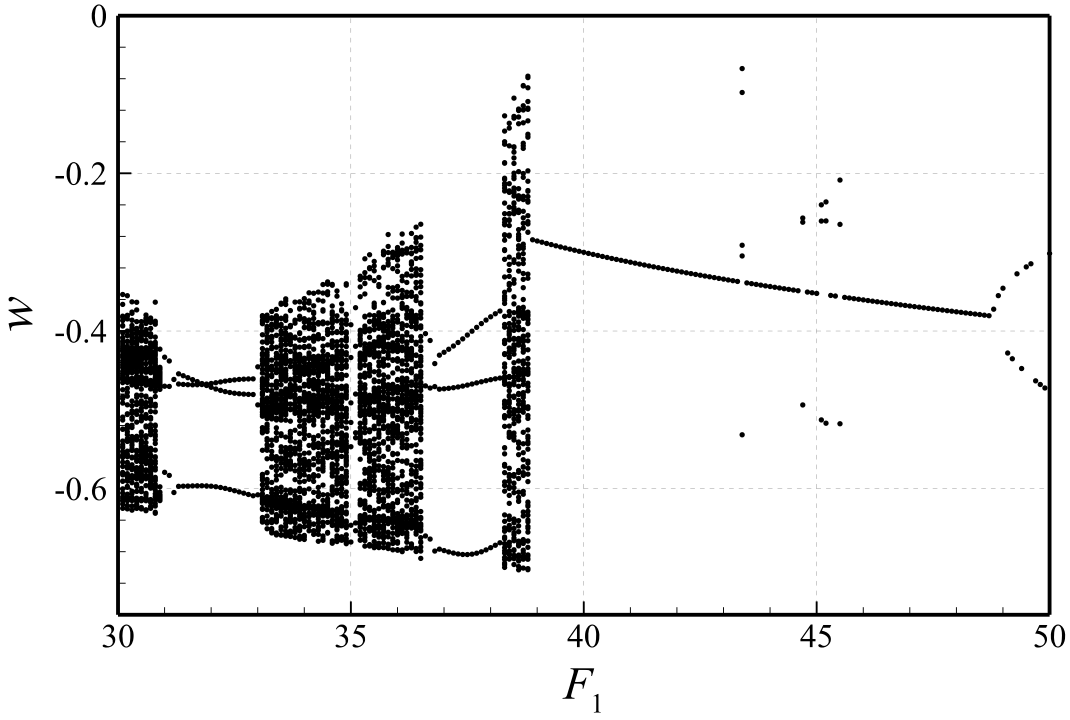

(b)

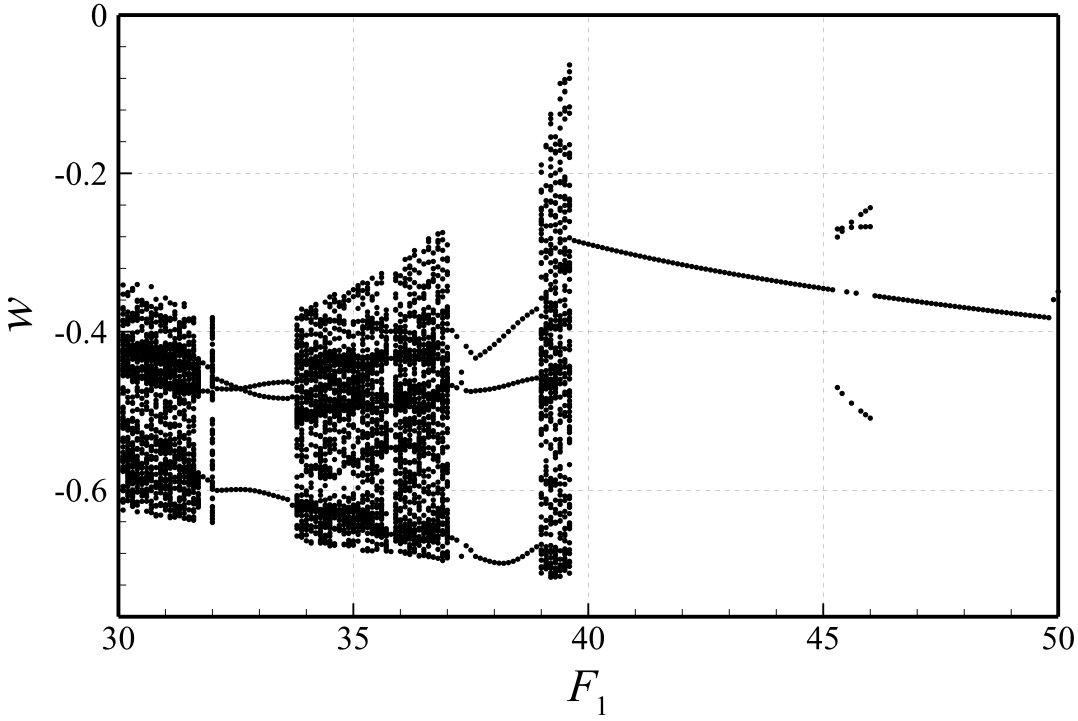

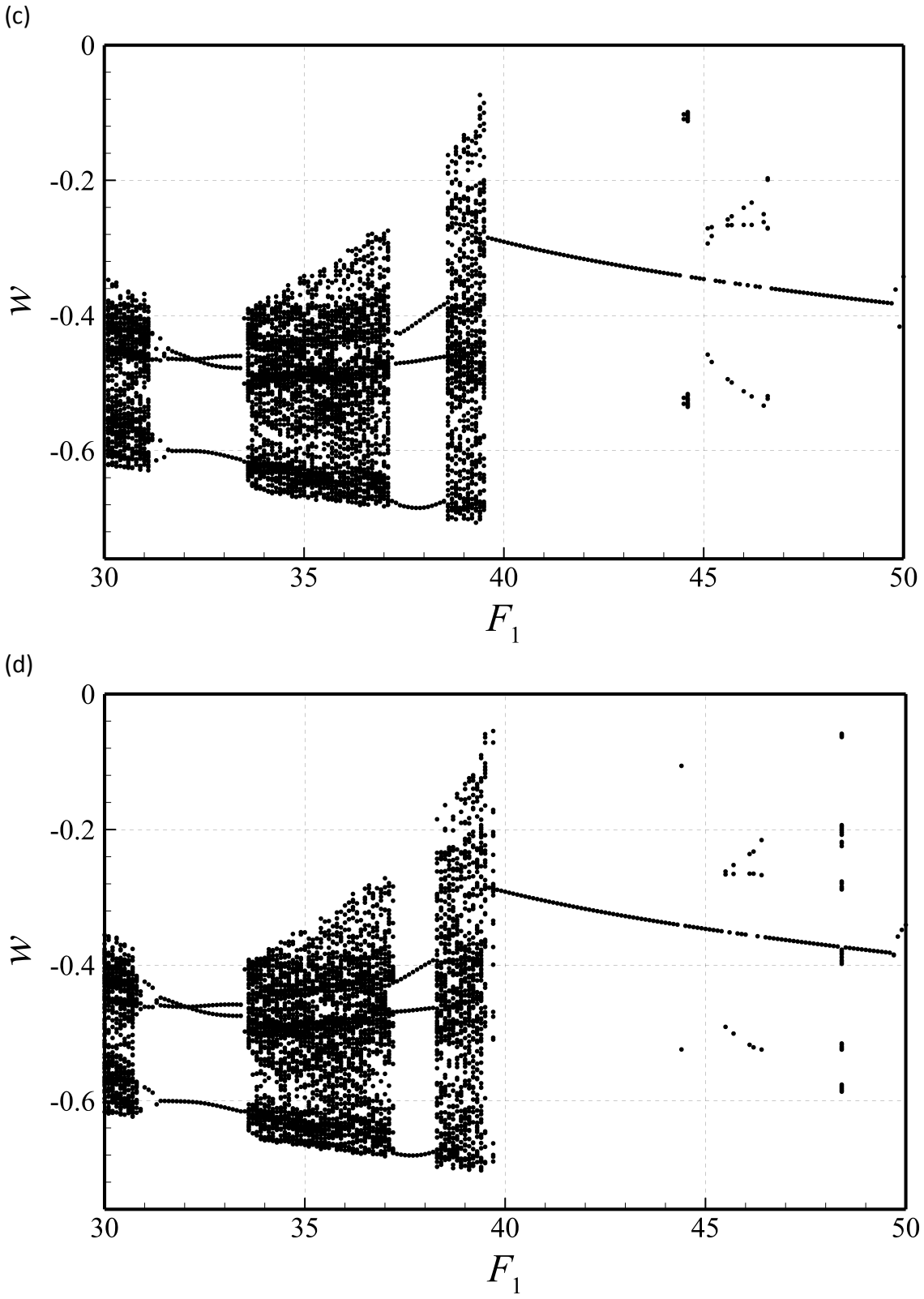

Figure 15: Bifurcation diagrams of Poincaré sections of the nanotube conveying nanofluid flow for $U = 4.10$: (a) 2-degree-of-freedom model; (b) 4-degree-of-freedom model; (c) 6-degree-of-freedom model; (d) 8-degree-of-freedom model.